CHALMERS
UNIVERSITY OF TECHNOLOGY

E Field [V/m]

1.1886E+004
6.4323E+003
3.4810E+003
1.8838E+003
1.0195E+003
5.5170E+002
2.9856E+002
1.6157E+002
8.7438E+001
4.7319E+001
2.5608E+001
1.3858E+001
7.4996E+000
4.0585E+000
2.1964E+000
1.1886E+000

Analysis, Construction and Evaluation of a Radial Power Divider/Combiner

Design of an 8-way TM_{020} Radial Cavity Divider/ Combiner with Coaxial Ports

Master's Thesis in Wireless, Photonics and Space Engineering

IDA KLÄPPEVIK

Analysis, Construction and Evaluation of a Radial Power Divider/Combiner

IDA KLÄPPEVIK

Analysis, Construction and Evaluation of a Radial Power Divider/Combiner
IDA KLÄPPEVIK

Department of Microtechnology and Nanoscience
Microwave Electronics Laboratory
Chalmers University of Technology
SE-412 96 Gothenburg
Telephone +46 31 772 1000

Cover: Cross section of the simulated electromagnetic field within a passive combiner/divider structure based on a resonant, cylindrical cavity, where coaxial probes excite the TM_{020} mode. The centred port at the bottom of the cavity is excited with 1 W.

Gothenburg, Sweden 2017

Analysis, Construction and Evaluation of a Radial Power Divider/Combiner

IDA KLÄPPEVIK

Department of Microtechnology and Nanoscience

Chalmers University of Technology

ABSTRACT

Radial N-way combiners and dividers are efficient and compact structures for power combining and dividing, which combines or divides the power of N inputs in one single step. The use of this method results in low losses and therefore presents an interesting alternative to often used combiner and divider networks, such as binary tree structures consisting of 2- or 3-way splitters.

In this thesis project, the construction of radial N-way cavity combiners and dividers is analysed and an 8-port TM_{020} cylindrical cavity combiner/divider with SMA-connector input and output ports is designed and fabricated. The characteristics of the fabricated prototype is evaluated and compared to the simulated design. The average return loss at the peripheral ports is higher than 18.4 dB and the return loss at the centre port is higher than 17.6 dB for a 10 % bandwidth around the centre design frequency of 3.1 GHz. The measured insertion loss is lower than 0.16 dB for the same band.

The divider and combiner are used in an active test setup with 8 InGaP HBT amplifiers, by which a study of degradation in the event of amplifier failure is performed. Methods to reach a more graceful degradation are discussed. The thesis report also presents a brief overview of different types of N-way combiners and a comparison between the characteristics of some published designs.

In conclusion, radial N-way combiners are a very attractive alternative for combining in high power systems due to their low-loss performance and the gradual loss of power in the event of amplifier failure. If they are used together with solid state power amplifiers, they can be used to replace other high power RF amplifier solutions such as the travelling wave tube amplifier.

PREFACE

In this thesis project, the concept of radial cavity power combiners has been investigated through theoretical studies and practical experiments. The thesis work resulted in two fabricated structures that were designed for power combining and dividing, and their functionality was tested and compared to simulated results.

The thesis project was carried out at Saab AB, with Magnus Isacsson (Saab AB) as supervisor and Dan Kuylenstierna (Chalmers University of Technology) as examiner. The work took place at Chalmers University of Technology and Saab AB from November 2016 to May 2017.

Firstly, I would like to express my sincere gratitude to my supervisor Magnus Isacsson for his dedicated supervision of this project, and for providing me with an introduction to practical engineering. Secondly, I would like to thank my examiner Dan Kuylenstierna for the guidance regarding the planning of the thesis project and the project report. I would also like to thank Niklas Einvall at Saab AB who made this thesis project possible.

Finally, I am very grateful towards the help and support from Theofilos Markopoulos, Sofia Berg, Ludvig Magnusson, Andreas Wikström, Per Agesund, Per Aulin, Sigrid Hammarqvist and other colleagues at Saab and all of my fellow thesis worker colleagues.

<div align="right">Ida Kläppevik, Gothenburg, May 2017</div>

TABLE OF CONTENTS

LIST OF FIGURES

LIST OF TABLES

1 INTRODUCTION

Today, military and space industries often demand technology with highest possible performance in combination with excellent reliability, as well as lowest possible size and weight. This also applies for radar and satellite communication, where the ambition to increase the range requires solutions to generate high output power at microwave frequencies. Robust, compact and high performing amplifier solutions are crucial constituents in radar and wireless communication systems.

Today, the travelling wave tube amplifier (TWTA) is dominating for RF frequencies since it is a well-tested and reliable solution, albeit with some drawbacks. TWTAs are expensive, require a considerable warm-up time and very high DC voltage, while being heavy and space consuming devices, especially for low-frequencies bands [1, 2].

However, the performance of solid state power amplifiers (SSPA) has improved rapidly over the decades with affordable and reliable devices as a result. One of the more promising technologies is the GaN transistor that shows very high break down voltage and high radiation tolerance [1]. Today, devices with output powers as high as hundreds of Watts are available [3]. Parallel to this technological development, the interest has grown in finding ways to use SSPAs for high power generation at microwave frequencies. The power limitation of the SSPA means that a number of SSPAs are required to generate high output powers. This is where efficient power combiners become crucial for the introduction of high frequent SSPA based high power amplifier solutions. Radial N-way combiners are compact, reliable and offer low-loss combination of power in one single step, which makes them suitable for the radar application.

The SSPAs in combination with power combining provides additional robustness as the system can operate even though one or more of the SSPAs stop working, albeit with decreased efficiency. This is called *graceful degradation* of power [4] and is a great advantage compared to the TWTA, for which the system fails completely if the TWTA breaks down. The SSPA based amplifier solution might also allow hot replacement, which means that broken amplifiers can be replaced in the radar or communication system during operation.

1.1 Aim of the project

The aim of this thesis project is to analyse the construction of radial N-way amplifiers and to design, fabricate and evaluate an N-way radial power divider and combiner structure. The divider and combiner are tested together with power amplifiers to verify the dividing and combining principle and to study the graceful degradation.

The thesis project focuses on resonant cavity dividers/combiners, and specifically aims to answer the following questions:

- How is an *N*-way radial power divider/combiner consisting of a resonant cavity constructed?
- How sensitive is the radial power combiner to inconsistencies in amplitude and phase in the input signals?
- What are the filter characteristics for the divider and combiner structure?
- How does failure of one amplifier affect
  - the matching at the other ports?
  - the coupling between input and output port?
  - the output power?
- How good return and insertion loss can be achieved?

The project is divided into four main parts: an initial literature study, analysis, design and fabrication of the combiner/divider structure, evaluation of the design and fabrication process and study of the graceful degradation for the designed combiner/divider.

1.2 Demarcations

The construction analysis and the design work will only cover radial power dividers and combiners based on a cylindrical resonant cavity, as the fabrication of prototypes of this sort is considered to be feasible within the limited time and resources of the project.

The power amplifiers used are not designed as part of the thesis project, as this would take too much time. Instead, existing amplifiers are used to evaluate the divider and combiner under realistic conditions.

2 THEORY

This section gives an overview of the theory behind *N*-way power combining, and goes through and compares different types of published designs. A reader skilled in the art is recommended to skip this sections and jump directly to section 2.2 and 2.3 for a brief introduction to power combiners and dividers and how they can be realized, since section 2.1 covers basic electromagnetic wave theory and fundamentals in microwave engineering. In the theory section, the word *combiner* will often be used to describe both combiner and divider structures as they in general are reciprocal passive networks that can be used in both applications.

2.1 Cylindrical Cavity Resonators

The cylindrical cavity is in all essential nothing else but a cylindrical waveguide shorted at both ends with conducting plates, forming a closed cylinder with conducting walls. This relation with cylindrical waveguides is also reflected in the electro-magnetic field expressions and modes, as will be discussed in section 2.1.1.

Resonance is a phenomenon occurring when a wave travels a certain distance and is thereafter reflected so that the incident and reflected waves interfere constructively. For waves travelling in the propagation direction in hollow waveguides this distance is $n \cdot \lambda / 2$, where n is any positive integer. For circular symmetries, electromagnetic fields are related to the Bessel function, which makes the criteria for resonance somewhat more mathematically complex. The circular symmetry of a cylindrical cavity leads to only two dimensions where resonance can occur: the height of the cylinder d (propagation direction) and the radius of the cylinder a (transverse direction). By careful design of the cylinder, specific resonant frequencies can resonate in the structure.
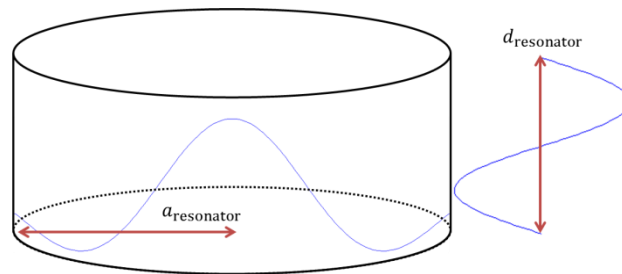
Figure 2-1. Schematic picture of a resonant cylindrical cavity with examples of resonant waves shown in height and radial dimensions.

The perfect, lossless resonator has no openings for excitation or signal output. Hence, waves with the resonant frequency will in theory resonate forever in the cavity if the surface material is perfectly conducting. However, as input and output ports are added to the cavity, addition of resistive and reactive elements disturbs the perfect resonator which may cause a shift of the resonant frequency and can cause losses. In real life, the walls will also introduce imperfections as metal is not perfectly conducting.

The parallel resonant circuit model [5] is a useful tool to describe the resonant cavity in an equivalent circuit, as shown in Figure 2-2. This model is convenient when the resonator should interact with surrounding networks or components, and can be used in impedance calculations and to relate the Q-factor to resistive and reactive components of the resonator [6].
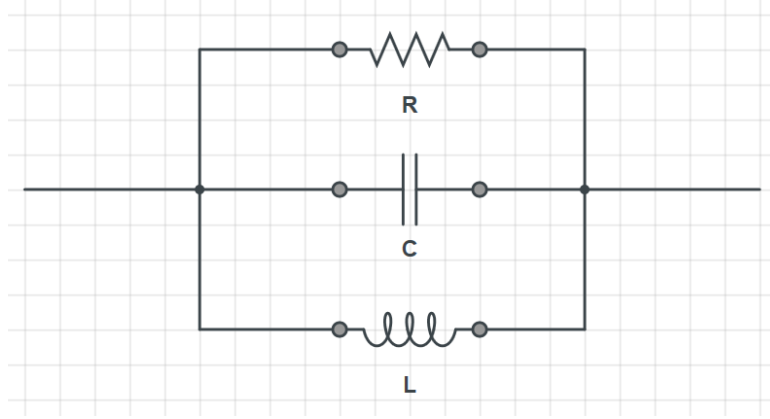
Figure 2-2. Lumped parallel resonant circuit.

2.1.1 Electromagnetic Fields in Cylindrical Cavities

The derivation of the field expressions for cylindrical cavities is simplified by the fact that the cylindrical cavity is a special case of circular waveguides. The shortened ends of the waveguide, creating the cavity, can simply be considered as two additional boundary conditions. The field expressions for a circular waveguide are listed in Table 2-1.

Table 2-1. Electric and magnetic field expressions for TE$_{nm}$ and TM$_{nm}$ modes
in a circular waveguide. [7]

Field	TE$_{nm}$ mode	TM$_{nm}$ mode
E_z	0	$(A \sin n\emptyset + B \cos n\emptyset) J_n(k_c\rho) e^{-j\beta z}$
H_z	$(A \sin n\emptyset + B \cos n\emptyset) J_n(k_c\rho) e^{-j\beta z}$	0
E_ρ	$\dfrac{-j\omega\mu n}{k_c^2 \rho}(A \cos n\emptyset - B \sin n\emptyset) J_n(k_c\rho) e^{-j\beta z}$	$\dfrac{-j\beta}{k_c}(A \sin n\emptyset + B \cos n\emptyset) J_n'(k_c\rho) e^{-j\beta z}$
$E_\emptyset$	$\dfrac{-j\omega\mu}{k_c}(A \sin n\emptyset + B \cos n\emptyset) J_n'(k_c\rho) e^{-j\beta z}$	$\dfrac{-j\beta n}{k_c^2 \rho}(A \cos n\emptyset - B \sin n\emptyset) J_n(k_c\rho) e^{-j\beta z}$
H_ρ	$\dfrac{-j\beta}{k_c}(A \sin n\emptyset + B \cos n\emptyset) J_n'(k_c\rho) e^{-j\beta z}$	$\dfrac{-j\omega\varepsilon n}{k_c^2 \rho}(A \cos n\emptyset - B \sin n\emptyset) J_n(k_c\rho) e^{-j\beta z}$
$H_\emptyset$	$\dfrac{-j\beta n}{k_c^2 \rho}(A \cos n\emptyset - B \sin n\emptyset) J_n(k_c\rho) e^{-j\beta z}$	$\dfrac{-j\omega\varepsilon}{k_c}(A \sin n\emptyset + B \cos n\emptyset) J_n'(k_c\rho) e^{-j\beta z}$

The fields are divided into transverse electric waves, denoted TE$_{nm}$, and transverse magnetic waves, denoted TM$_{nm}$, where "transverse" means that no field exists in the propagation direction, z. All expressions contain the Bessel function of the first kind, $J_n(k_c\rho)$, or its derivative, $J_n'(k_c\rho)$. The Bessel function has m-1 extreme points, and a plot describing the behaviour of the Bessel function is displayed in Figure 2-3.

4
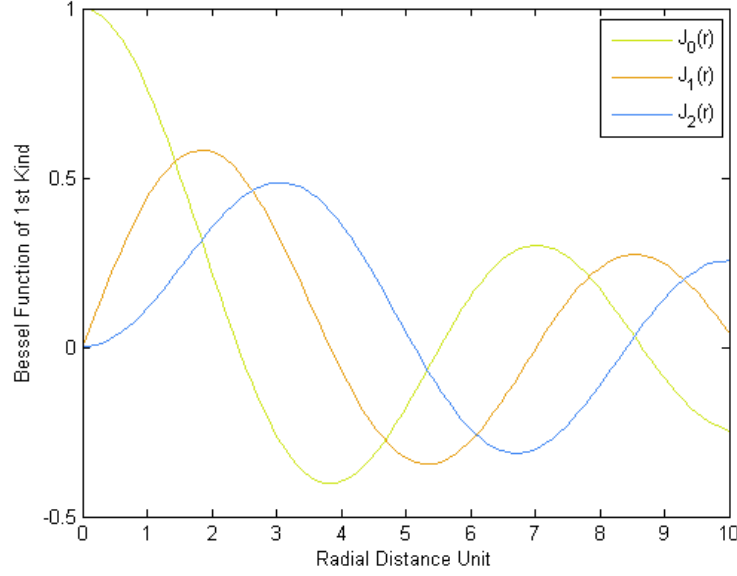
Figure 2-3. The behaviour of the Bessel function of first kind.

The circular waveguide field functions satisfy the boundary conditions for the side wall in the cylindrical resonator when $J_n(k_c\rho) = 0$ or $J'_n(k_c\rho) = 0$. For TE$_{nm}$ modes, the root is often called p'_{nm} so that $J_n(p'_{nm}) = 0$, and similarly, the root for TE$_{nm}$ modes is often called p_{nm} so that $J_n(p_{nm}) = 0$. Some of the values of the roots are listed in Table 2-2 below.

Table 2-2. Values of p'_{nm} and p_{nm} for TE$_{nm}$ and TM$_{nm}$ modes respectively, in circular waveguides.

n	p'_{n1}	p'_{n2}	p'_{n3}	p_{n1}	p_{n2}	p_{n3}
0	3.832	7.016	10.174	2.405	5.520	8.654
1	1.841	5.331	8.536	3.832	7.016	10.174
2	3.054	6.706	9.970	5.135	8.417	11.620

To accurately describe the field in a cylindrical cavity, the shorted planes at $z = 0, d$ must be accounted for. Pozar [7] does this, by writing the expression for the transverse fields as below

$$\vec{E}_t(\rho, \phi, z) = \vec{e}(\rho, \phi)\left(A^+ e^{-j\beta_{nm}z} + A^- e^{+j\beta_{nm}z}\right) \tag{2.1}$$

where the two functions $\vec{e}(\rho, \phi)$ and $\left(A^+ e^{-j\beta_{nm}z} + A^- e^{+j\beta_{nm}z}\right)$ represents the transverse variation of the mode and the amplitudes of the forward and backward wave respectively. These functions are both affected by the boundary condition set by the shorted planes: $\vec{E}_t = 0$ for $z = 0, d$. The solution to (2.1) with these boundary conditions gives that the forward and backward wave amplitude must be inversely related as $A^+ = -A^-$, which implies that $A^+ \sin(\beta_{nm}d) = 0$. The latter relates the dimensions of the cavity to the modes that can exist in it since the solution to the equation is $\beta_{nm}d = l\pi$ where l is any integer ≥ 0 [7].

2.1.2 Resonant Modes

As discussed in the previous section, a number of modes with different mode indices nm can propagate in waveguides. For the cylindrical cavity, standing waves can also occur in the

propagation direction leading to yet another mode index. Hence, cylindrical cavities can support fields such as TE_{nml} and TM_{nml}.

The relation between resonant frequencies, dimensions and mode indices is derived in [7], by use of the expression for the propagation constant

$$\text{TE:} \qquad \beta_{nm} = \sqrt{k^2 + \left(\frac{p'_{nm}}{a}\right)^2} \qquad (2.2)$$

$$\text{TM:} \qquad \beta_{nm} = \sqrt{k^2 + \left(\frac{p_{nm}}{a}\right)^2} \qquad (2.3)$$

where $k = \omega\sqrt{\mu\varepsilon}$. By rearranging (2.2) and (2.3), expressions for the cut off-frequencies for the different modes are expressed as

$$\text{TE}_{nml}: \qquad f_{nml} = \frac{c}{2\pi\sqrt{\mu_r\varepsilon_r}} \sqrt{\left(\frac{p'_{nm}}{a}\right)^2 + \left(\frac{l\pi}{d}\right)^2} \qquad (2.4)$$

$$\text{TM}_{nml}: \qquad f_{nml} = \frac{c}{2\pi\sqrt{\mu_r\varepsilon_r}} \sqrt{\left(\frac{p_{nm}}{a}\right)^2 + \left(\frac{l\pi}{d}\right)^2}. \qquad (2.5)$$

2.1.3 Q-factor of Resonators

The quality factor (Q-factor) is a measure of the loss in a resonator. It is defined as the ratio between stored energy W and power losses P_l in the resonator,

$$Q = \frac{W\omega}{P_l} \qquad (2.6)$$

and it is also inversely related to the bandwidth of the system. Cylindrical cavity resonators often have high Q-factor [8].

The stored energy of a cavity is calculated by summing up either the time average electric or time average magnetic energy, since they are equal at resonant frequencies [8]. They are both calculated from the field expressions for a circular waveguide in Table 2-1 and the expressions for the time average electrical energy and the power losses are [8]

$$W = 2W_e = \frac{\varepsilon}{4} \iiint |E_r|^2 + \left|E_\phi\right|^2 r\, d\phi\, dr\, dz \qquad (2.7)$$

$$P_l = \frac{R_s}{2} \iint_{walls} \left|\vec{H}_{\text{tan}}\right|^2 dS. \qquad (2.8)$$

where R_s is the surface resistance of the cavity, determined by skin depth δ_s and conductivity σ as $R_s = 1/\delta_s\sigma$ [7]. By insertion of the field expressions from Table 2-1, the expression for the Q-factor is found to be [8]

$$Q = \frac{W\omega}{P_l} = \frac{\lambda_0}{\delta_s} \frac{\left[1 - \left(\frac{n}{p'_{nm}}\right)^2\right]\left[(p'_{nm})^2 + \left(\frac{l\pi a}{h}\right)^2\right]^{3/2}}{2\pi\left[(p'_{nm})^2 + \frac{2a}{h}\left(\frac{l\pi a}{h}\right)^2 + \left(1 - \frac{2a}{h}\right)\left(\frac{nl\pi a}{p'_{nm}h}\right)^2\right]} \tag{2.9}$$

for the TE-mode. By replacing p'_{nm} with p_{nm}, the Q-factor for the TM-modes is found. As mentioned earlier, the Q-factor and the bandwidth of the resonator are inversely related to each other [8]

$$Q = \frac{1}{BW}. \tag{2.10}$$

2.1.4 The Scattering Matrix for Microwave Networks

When working with microwave networks, the tools and models usually applied on low frequency networks cannot always be applied, and other ways to describe and measure a circuit must be used. When the wavelength of the high frequency signal is comparable with the size of the components and the media of transmission, the field expansions in the component must be considered. This means that the concept of current and voltage are different in a microwave circuit compared to the low frequency circuit.

The equivalent current and voltage definitions for waveguides are based on the expressions for electromagnetic waves in section 2.1.1, which means that each mode will have its individual equivalent current and voltage. A result of the distributed approach is also that reflections have to be considered for unmatched components, which leads to forward and backward waves. By writing the transverse field expression [7] as in (2.1), the equivalent current and voltage can be introduced

$$\begin{aligned}\vec{E}_t(\rho,\phi,z) &= \vec{e}(\rho,\phi)\left(A^+ e^{-j\beta_{nm}z} + A^- e^{+j\beta_{nm}z}\right) \\ &= \frac{\vec{e}(\rho,\phi)}{C_1}\left(V^+ e^{-j\beta_{nm}z} + V^- e^{+j\beta_{nm}z}\right)\end{aligned} \tag{2.11}$$

$$\begin{aligned}\vec{H}_t(\rho,\phi,z) &= \vec{e}(\rho,\phi)\left(A^+ e^{-j\beta_{nm}z} + A^- e^{+j\beta_{nm}z}\right) \\ &= \frac{\vec{e}(\rho,\phi)}{C_2}\left(I^+ e^{-j\beta_{nm}z} - I^- e^{+j\beta_{nm}z}\right).\end{aligned} \tag{2.12}$$

and defined in a more useful manner as

$$V(z) = V^+ e^{-j\beta z} + V^- e^{j\beta z} \tag{2.13}$$

$$I(z) = I^+ e^{-j\beta z} - I^- e^{j\beta z}. \tag{2.14}$$

The definition of $V(z)$ and $I(z)$ is chosen so that the characteristic impedance Z_0 is defined as $Z_0 = V/I$.

A common situation to use the equivalent voltage and current is in multiport microwave networks. For these networks, impedance and admittance may differ between all ports

combinations. A convenient way to describe the impedance and admittance of a microwave system is to create impedance matrices $[Z]$ and admittance matrices $[Y]$

$$[V] = [Z][I] \quad \Rightarrow \quad \begin{bmatrix} V_1 \\ \vdots \\ V_N \end{bmatrix} = \begin{bmatrix} Z_{11} & \cdots & Z_{1N} \\ \vdots & \ddots & \vdots \\ Z_{N1} & \cdots & Z_{NN} \end{bmatrix} \begin{bmatrix} I_1 \\ \vdots \\ I_N \end{bmatrix} \tag{2.15}$$

$$[I] = [Y][V] \quad \Rightarrow \quad \begin{bmatrix} I_1 \\ \vdots \\ I_N \end{bmatrix} = \begin{bmatrix} Y_{11} & \cdots & Y_{1N} \\ \vdots & \ddots & \vdots \\ Y_{N1} & \cdots & Y_{NN} \end{bmatrix} \begin{bmatrix} V_1 \\ \vdots \\ V_N \end{bmatrix} \tag{2.16}$$

where each element $Z_{ij} = \frac{V_i}{I_j}$ or $Y_{ij} = \frac{I_i}{V_j}$ represents the impedance or admittance between port i and j [7].

Another matrix model that can be defined from the equivalent voltage and current is the scattering matrix

$$[S] = \begin{bmatrix} S_{11} & \cdots & S_{1N} \\ \vdots & \ddots & \vdots \\ S_{N1} & \cdots & S_{NN} \end{bmatrix}. \tag{2.17}$$

The elements of the scattering matrix are known as S-parameters

$$S_{ij} = \frac{V_i^-}{V_j^+} \tag{2.18}$$

and is a measure of how an incident wave is scattered when travelling from port j to i, or is incident upon a port i [7]. In the latter case, the S-parameter is simply S_{ii}.

For reciprocal networks

$$[S] = [S]^t \tag{2.19}$$

and for lossless networks [8]

$$\sum_{k=1}^{N} |S_{ki}|^2 = 1 \tag{2.20}$$

$$\sum_{k=1}^{N} S_{ki} S_{kj}^* = 0. \tag{2.21}$$

2.1.5 Impedance of Cavity Resonators

In the introduction to this chapter, it was stated that a cavity resonator can be modelled as the parallel resonant circuit. The calculation of impedance and admittance for such a circuit is a matter of application of circuit theory

$$Y(\omega) = \frac{1}{R} + \frac{1}{j\omega L} + j\omega C, \tag{2.22}$$

$$Z = (Y)^{-1} = \left(\frac{1}{R} + \frac{1}{j\omega L} + j\omega C\right)^{-1}. \tag{2.23}$$

The parallel resonant circuit model is related to the real resonant cavity by the relationship between the Q-factor and the elements of the circuits [5], stating that

$$Q = \omega_0 RC \tag{2.24}$$

where ω_0 is the resonant frequency [7]

$$\omega_0^2 = \frac{1}{LC}. \tag{2.25}$$

From these definitions, it is possible to rephrase the impedance for the cylindrical cavity resonator as [6]

$$Z = -\frac{\frac{j\omega}{C}}{\omega^2 - \omega_0^2\left(1 + \frac{j}{Q}\right)}. \tag{2.26}$$

2.1.6 Excitation of Cavities

There are a number of aspects to consider when a resonator should be excited; the coupling between the resonator and the feed, the frequency of the inserted signal and where the signal is inserted, to mention a few. In order to excite a certain resonant mode in a cavity, the field from the excitations should support the field of the resonant mode. This means feeding the field where it should have a maximum, and by that feeding a resonant field. An example of this is the excitation of the TM_{020} mode in a cylindrical cavity resonator in [9].

The electromagnetic wave needs to be be inserted into the cavity in some way to feed the resonator, which can be done by penetrating the cavity walls with some sort of wave guiding device. A resonant system can have a number of ports for excitation or signal tapping that will affect the resonant performance of the cavity, as mentioned in section 2.1. In this section, any type of usage of ports in the cavity will be called excitation.

A variety of different cavity excitations exist in literature, but the most common means of excitations are coaxial waveguides, probes, hollow waveguide apertures, and microstrips or striplines inserted into the cavity. The choice of excitation method can be based upon properties such as frequency range, power levels or losses, but could also be made considering practicalities such as volume restrictions or what other microwave networks or equipment the resonator should be connected to. In this project, waveguide excitation through apertures and coaxial probes will be discussed.

A useful way to model the effect of the addition of excitation ports is to add their equivalent circuits to the parallel resonant circuit, and calculate the behaviour of the complete circuit with circuit theory. For example, the coupling between the excitation feed and the resonator

can be calculated, which is of interest for maximum power transfer where critically coupled excitations are desirable [7].

2.2 Power Dividing/Combining

Power dividing and combining is a common need in microwave engineering, and is often realized through usage of components such as simple T-junctions, Wilkinson dividers or hybrid couplers [7]. As the components are passive, they can be used as combiners as well as dividers. A divider or combiner should ideally divide the power perfectly with no insertion or return losses, or any unwanted leakage between ports on "the same side". Assuming that a three-port divider is reciprocal, lossless and has perfectly matched ports, the scattering matrix will be

$$[S] = \begin{bmatrix} 0 & S_{12} & S_{13} \\ S_{12} & 0 & S_{23} \\ S_{13} & S_{23} & 0 \end{bmatrix} \tag{2.27}$$

where the diagonal elements are zero due to the matched ports. The rules about scattering parameters for lossless networks (2.20)-(2.21) gives the following equations:

$$|S_{12}|^2 + |S_{13}|^2 = 1, \qquad\qquad S_{23}S_{13}^* = 0,$$

$$|S_{12}|^2 + |S_{23}|^2 = 1, \qquad\qquad S_{12}S_{23}^* = 0, \tag{2.28}$$

$$|S_{13}|^2 + |S_{23}|^2 = 1, \qquad\qquad S_{13}S_{12}^* = 0.$$

However, the three expressions to the right in (2.28) will contradict the expressions to the left in the same equation. It is not physically possible to have perfect matching at all ports and a reciprocal and lossless system simultaneously [7].

2.2.1 *N*-port Power Combining

Power division and power combining play essential part in high power microwave networks, when amplification is to be achieved with solid state power amplifiers (SSPAs). Traditionally, SSPAs has not been used in high power amplifications due to their limited output power. Instead, more powerful amplifiers such as travelling wave tube (TWT) amplifiers have been used. However, SSPA:s offer great advantages over TWTs due to their small size, short warm-up time, high efficiency and easy replacement in the case of failure [2].

To increase the power level of SSPAs, power dividers are normally used to split the incoming signal into *N* signals that each will be amplified separately by its own designated SSPA. The *N* amplified signals are then recombined in a power combiner, resulting in a high power output. The procedure is illustrated in Figure 2-4.
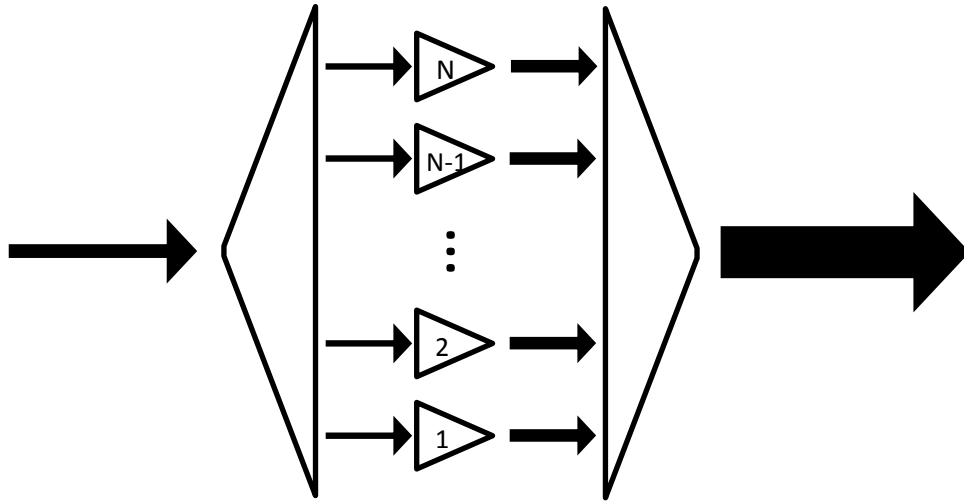
Figure 2-4. Schematic display of power combining/dividing.

Most structures are designed to be passive and reciprocal, and can therefore be used as both dividers and combiners. For practical reasons, the word *combiner* will be used for the structure described in this section of the report, and theory will if nothing else is stated also apply to dividers.

Power combining of radio frequency signals can be realized with several different techniques and structures. Different power combining techniques will be discussed further in section 2.2.2 below.

2.2.2 Power Combining Techniques

N-port combination of RF signals can be achieved in many different ways, all of which can be sorted based on a fundamental property: if they are one-step or multiple-step structures. Russel [4] provides an overview in different combining techniques, albeit somewhat dated as new technological advantages have been made since the publication of the article.

The multiple step combiners are typically based on a network of 3-port combiners, arranged in a binary corporate structure, also known as tree structure [4] as seen in Figure 2-5. This structure is often seen in microstrip applications. The 3-port combiners can have isolated ports that prevent leakage which means that this structure can be very efficient in theory, when different 3-port combiners are assumed to be perfectly matched and lossless. In reality, however, losses will always occur and will be added in each step, limiting the efficiency of the structure to a maximum number of steps before the efficiency becomes too low [4].
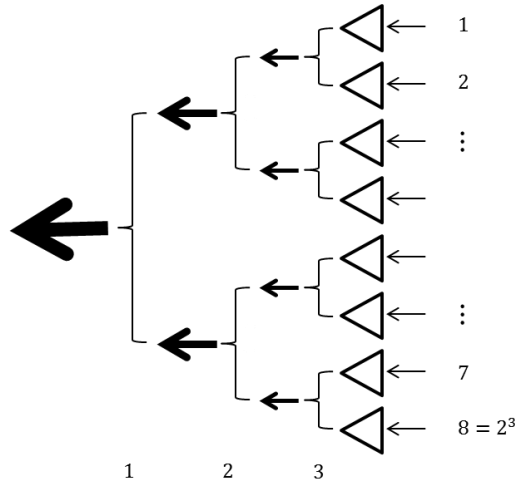
Figure 2-5. Schematic display of binary tree structure with 3 steps and $2^3 = 8$ solid state power amplifiers.

The multiple step combiners can also be arranged as serial combiners, also known as chain combiners. Chain structures consist of any number of combiners connected in serial, matched to the structure with coupling coefficients specific for the position of the combiner [4]. One of the benefits with the structure is the fact that additional combiners can be added to the structure as long as it fulfils the coupling coefficient requirements. Drawbacks are high losses and difficulties to realize the coupling coefficients for a high number of combiners [4].

N-way combining structures differ from the previous two families since they apply 1-step combination. These are all structures where the input ports are connected in parallel to a combining node. By this principle, the matching losses decrease significantly compared to the tree structure combiners. Other advantages of the *N*-way combiners are graceful degradation of output power in the case of amplifier failure and the possibility of hot replacements, meaning that malfunctioning parts of the systems can be replaced during operation. *N*-way combiners can be radial as well as non-radial, where the radial *N*-way combiner is dominating due to its clever usage of space which allows for a higher number of ports to be combined [10]. Section 2.3 presents the different methods for realizations of radial *N*-way combiners as well as some examples from literature.

The thesis project will cover the construction an *N*-way combining structure based on a resonant cavity.

2.3 Methods of Realization of Radial *N*-way Combiners

The *N*-way combiners can be divided into three sub-groups: cavity-based combiners, non-cavity-based combiners and spatial combiners. *N*-way combiners can sometimes benefit from a mix between different technologies, and it is not always trivial to sort them into the structure in Figure 2-6. The choice between different types of *N*-way combiners is made depending on requirements such as wanted bandwidth, efficiency, size, isolation, tolerance of amplitude and phase errors and graceful degradation [10]. The input and output ports of a divider and combiner should also be compatible with the system where the amplifier solution should be used and the occurring power levels. For very high output power, e.g. in radar applications that requires several kW, a waveguide output from the combiner might be the only feasible solution, which in turn might affect the choice of divider and combiners structure.

12
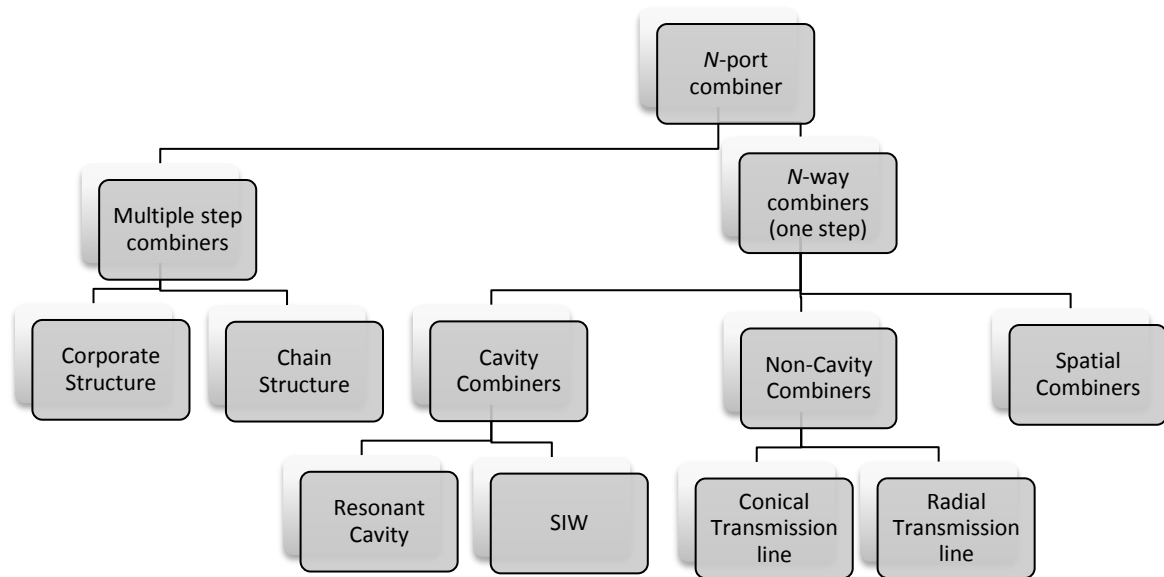
Figure 2-6. Different *N*-port power combining techniques arranged in a tree structure.

Even though *N*-way combiners has been seen in articles since at least the 70's [11, 9, 12, 13] it must be considered a relatively young technology that has not been developed enough to challenge the well-established corporate structures in industrial scale. However, since 2000, new designs based on radial transmission lines and spatial technology are beginning to show impressing performance [14, 15].

A brief presentation of the different technologies used for combiners and dividers are listed below with some interesting examples and a comparison between published designs.

2.3.1 Radial Cavity-Based Combiners

Cavity based radial power combiners guide the electromagnetic wave through the medium with lowest loss of all: free space. There are two common types of radial cavity combiners [10]: combiners based on resonant cylindrical cavities and combiners based on substrate integrated waveguides (SIW), where the latter are a result of implementation of the relatively new SIW technology [16] and therefore not very widespread.

The ground principle of the cavity combiners is very simple: a circularly symmetric field with a maximum in the centre point is excited in the cavity by carefully positioned excitation ports, and the combined signal from the many input ports is tapped out in the centre port. A cylindrical cavity can be excited with almost any type of waveguide: hollow waveguides, microstrip patches, coaxial cables, probes etc. To improve bandwidth and matching, additional sub-cavities or probe designs can be added to the construction, which is done in [12]. Another factor that affects the efficiency of the combiner is the leakage between input ports that occurs due to spurious modes in the cavity. In principle, it can be prevented by slits or barriers that suppress the unwanted modes. However, in most designs no precautions to improve input isolation are taken. An interesting example of a cylindrical cavity-based combiner is [17], where a complete combiner SSPA amplifier-system is presented. The amplifier circuits are mounted as trays at the periphery of the divider and combiner, which

allows separate testing of each individual port and gives an idea of what a hot replacement-solution could look like.

The radial cavity-based combiners are well-suited for narrowband solutions as the cavity or waveguide is designed for a certain resonant frequency. On the plus side, they offer relatively compact solutions with low intermediate losses. A comparison between typical cavity-based combiners is listed in Table 2-3. Constructions with more than 16 ports are seldom found in literature for this technology. Whether the reason for this is that the technology does not perform well for a high number of ports or not is unknown.

Table 2-3. Comparison between selected radial cavity-based combiner designs.

Author	Matsumura et al (1987) [9]	Matsumura et al (1988) [18]	Tokumitsu et al (1984) [12]	Ravindra et al (2015) [19]	Shan et al (2009) [20]	Li et al (2014) [21]	Song et al (2008) [22]	Song et al (2008) [14]	Denoual et al (2008) [17]	He et al (2016) [23]	Gharekand (2014) [24]
Technology	Cylindrical cavity with slits	Cylindrical cavity with slits and sub-cavity	Cylindrical cavity with sub-cavity	Cylindrical cavity	Cylindrical cavity	Octagonal Cavity	Cylindrical waveguide	SIW	Coaxial cavity	Cylindrical Cavity	Cylindrical Cavity
Combined ports	8	4	8	6	8	8	8	8	16	8	16
Port Interface — In	Coaxial	Rectangular waveguide	Coaxial	Microstrip	Microstrip	Rectangular waveguide	Coaxial	Probe	Waveguide	Probe	Coaxial
Port Interface — Out	Coaxial	Rectangular waveguide	Coaxial	Rectangular waveguide	Coaxial	Coaxial	Probe	Probe	Coaxial	Probe	Waveguide
f_0	12 GHz	14 GHz	6 GHz	9.65 GHz	14 GHz	10 GHz	8 GHz	5.25 GHz	18 GHz	29.5 GHz	4.7 GHz
Insertion Loss (f_0)	0.45 dB	0.25 dB	0.2 dB	0.3 dB	0.1 dB	1.8 dB	1 dB	0.2 dB	2 dB	--	0.7 dB
Return Loss (f_0)	--	--	18 dB	20 dB	20 dB	15 dB	15 dB	30 dB	12 dB	15 dB	22 dB
BW	RL>10 dB: 1.13 GHz	IL<0.1 dB: 500 MHz	IL<0.2 dB: 600 MHz	IL<0.3 dB: 200 MHz	RL>20 dB: 1.9 GHz	RL>15 dB: 4 GHz	RL>15 dB: 7 GHz	RL>15 dB: 500 MHz	RL>12 dB: 4.5 GHz	RL>15 dB: 7 GHz	IL<0.7 dB: 600 MHz

2.3.2 Radial Non-Cavity-Based Combiners

Non-cavity-based radial combiners are often made of microstrip or stripline, which is convenient due to their compatibility with integrated circuits, for example MMIC, that allows dense combiner solutions. To not have to match different technologies in at least one port might save losses. An advantage with the microstrip technology is that matching and isolation can be managed with lumped, off-the-shelf components as in [25], which makes this technology suitable for solutions with high isolation requirements. The large radial transmission line that is used to combine the input signals limits the bandwidth of the combiner [10], which together with previous listed characteristics makes this combiner type suitable for narrow bandwidth combiner in microstrip systems. One feature that makes the microstrip and stripline combiners attractive are the many design methods available, for example the ones presented in [25] and [15].

Another type of non-cavity-based radial combiners is the conical transmission line combiners, as presented in [26]. They transform a coaxial port to a funnel-shaped cavity, with a tapering design to match the coaxial input ports to the single combination port.

Table 2-4. Comparison between selected radial non-cavity-based combiner designs.

Author	Belehoubek *et al* (1986) [13]	Fathy *et al* (2006) [25]	Jain *et al* (2014) [15]	Dirk (2008) [26]
Technology	Radial transmission line	Radial transmission line	Radial transmission line + coaxial	Conical Transmission Line
Combined ports	30	30	16	10
Port Interface — In	Coaxial	Coaxial	Coaxial	Coaxial
Port Interface — Out	Coaxial	Microstrip/ Coaxial	Coaxial	Tapered Coaxial
f_0	11 GHz	12.5 GHz	505.8 MHz	10
Insertion Loss (f_0)	0.4 dB	0.55 dB	0.1 dB	0.28 dB
Return Loss (f_0)	--	16 dB	22 dB	18.5 dB
BW	IL < 0.5 dB: 600 MHz	--	RL>15 dB: 40 MHz	RL > 18.5 dB: 4.7 GHz

2.3.3 Spatial Combiners

A technology developed over the last two decades is the spatial power combiner [27], which usually is presented as complete amplification systems with divider, amplifier and combiner in one complete network. As the spatial combiners guide the signals through air, and use antenna interfaces, the intermediate losses are very low. However, antenna coupling factors may introduce losses. The spatial combiners provide a large bandwidth, and is often used for high frequencies, making them suitable for applications within communication, where high

data transfer is of importance [28]. H. Javadi-Bakhsh and R. Faraji-Dana published a spatial combiner with 20 elements [27] with tray amplifiers in 2014 with fin-line antenna elements that show the typical principle behind spatial combiners.

3 DIVIDER AND COMBINER DESIGN AND FABRICATION

In this thesis project, a full setup of an SSPA amplifier solution is designed and fabricated, and then evaluated. This section of the report will cover a conceptual study of cylindrical cavity combiners and dividers, design of the divider and combiner prototype and fabrication of the test setup.

3.1 Conceptual Study of Cylindrical Cavity Dividers and Combiners

A simple, conceptual design of a cavity combiner with a circular centre port and rectangular peripheral ports was developed with inspiration from [9] and [18]. The structure was used to study the impact of different design parameters.

3.1.1 Cylindrical Cavity

The combiner structure is based on a cylindrical resonant cavity where a chosen mode TM_{0m0} is excited. The mode index m should be two or higher since m=1 does not have any extreme point in the E_z-field, and should be chosen in relation to the number of peripheral ports and the bandwidth of the combiner or designer [9]. In this thesis project, structures based on the TM_{020} modes are studied. Equation (2.4) is used to determine the wanted radius of the cavity in order for to it to support a resonant frequency f_r for the mode in question.

In order for the cavity height related mode index l to be zero, a limitation is set for the cavity height d to never be $\lambda/2$ or higher. This should apply to the highest frequency in the wanted frequency band, with a margin of at least 10 %. With this rule of thumb applied to the frequency interval of 2.9 GHz-3.3 GHz, the height of the resonant cavity should be $d < 40.9$ mm.

Figure 3-1 shows a mode chart where the TE_{nm0} and TM_{nm0} modes from the listed values of nm from Table 2-2 are plotted. This can be used to determine if any other – unwanted – modes might resonate as a result of the excitation of the wanted mode. Unwanted modes are called spurious modes and there are a number of ways to suppress them. These will not be discussed within this thesis projects, but the interested reader finds an example of how mode suppression can be done in a resonant cavity combiner in [9].
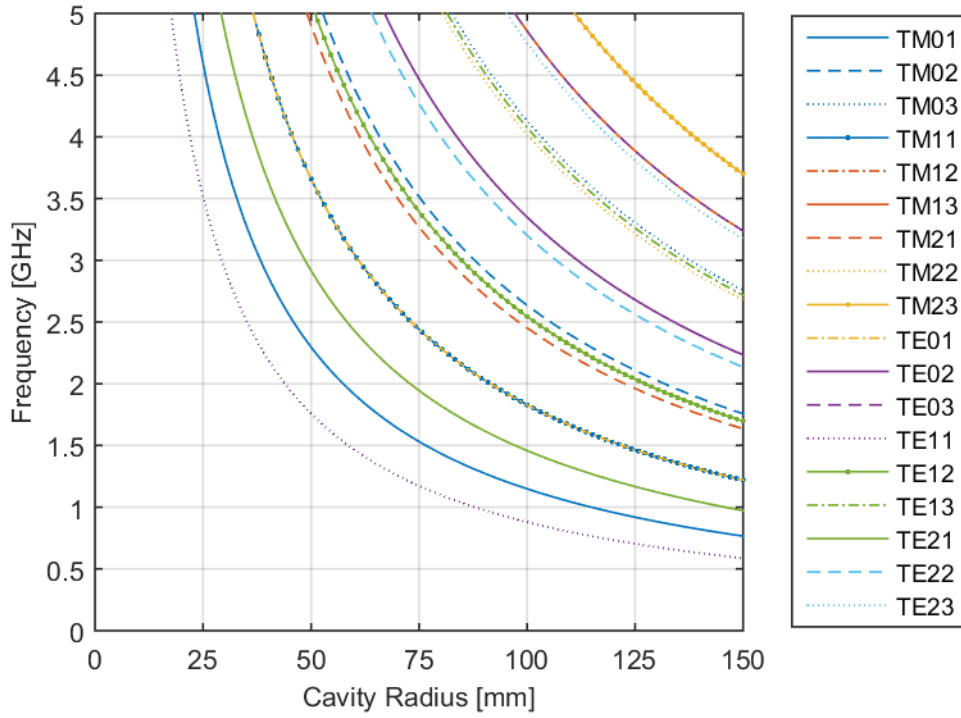
Figure 3-1. Resonant modes in the cylindrical cavity calculated from the solutions to the Bessel function from Table 2-2. Some of the modes overlap. The resonant modes closest to TM_{020} are TM_{210} and TE_{120}.

From (2.4), it is clear that the resonant frequency should not be affected by variation of cavity height d when $l = 0$. However, another important property of the resonant cavity will vary with cavity height: the input impedance. Montgomery, Dicke and Purcell [5] describe the input impedance of a cavity by an example containing a shorted waveguide excited with a waveguide iris aperture. Exclusion of the impedance contribution from the iris gives the input impedance for the resonator

$$Z_{in} = Z_0 \tanh([\alpha + j\beta]l) \tag{3.1}$$

where the attenuation coefficient α and the propagation constant β are fixed values for a certain mode, leaving the cavity height l as only variable. Figure 3-2 below shows how the normalized input impedance is affected by the cavity height, with the resistive and reactive components plotted as separate graphs. The resistive part is close to unchanged while the reactive component varies as the tanh-function, which implies that the cavity height can be used as a tuning parameter for impedance matching. The detailed calculation of (3.1) is found in APPENDIX A
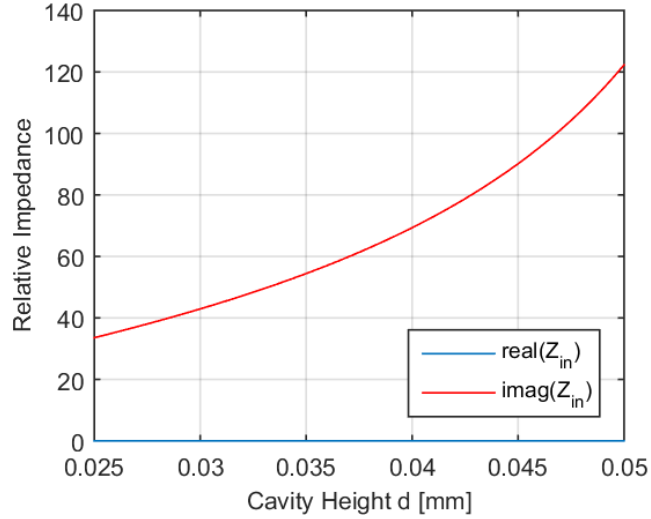
Figure 3-2. Normalized real (resistive) and imaginary (reactive) impedance variation with height for aTM$_{020}$ cylindrical cavity combiner.

In Figure 3-3, the results from a HFSS simulation of a cylindrical cavity with a centred input and an identical, opposite output circular waveguide are displayed. The cavity height was varied resulting in a clear change of the scattering parameters, as predicted by (3.1).
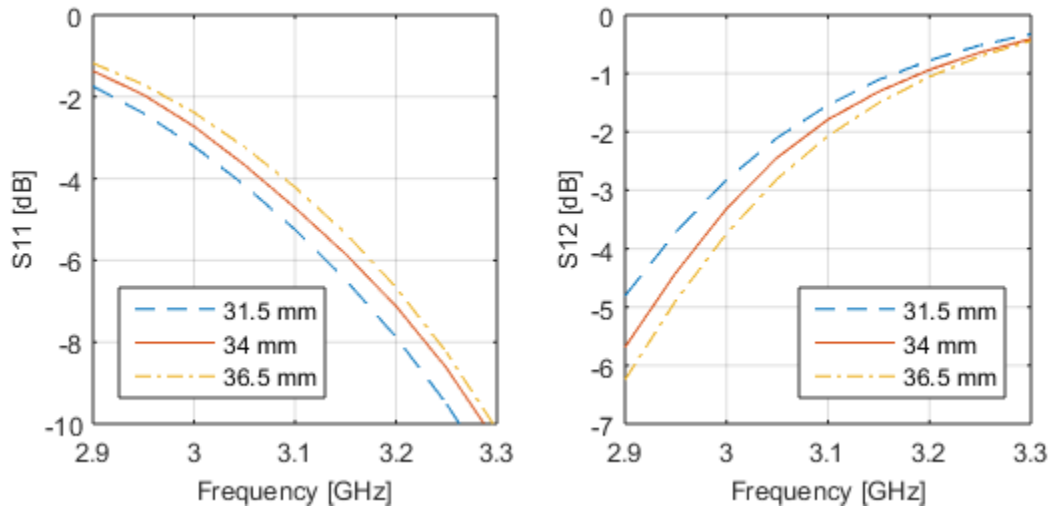
Figure 3-3. Reflection and transmission scattering parameter for a cylindrical cavity with two symmetric centre ports positioned opposite to each other. The cavity height is varied between three different heights: 31.5 mm, 34 mm and 36.5 mm.

3.1.2 Position and Choice of Peripheral and Centre Ports

Every radial combiner has a set of peripheral ports where signals are inserted into combiners, and a centred port where the combined signal can be tapped out. The ports should guide the correct frequencies and allow coupling between the combiner and the surrounding microwave network with as small losses as possible.

For the conceptual design, rectangular waveguides are used as peripheral ports and a circular waveguide is used as a centre port, as in [18]. Waveguides are convenient for analysis in

HFSS as it is easy to display and analyse fields in hollow waveguides in the software. The length of the waveguides was set to an arbitrary value $5\lambda/2 < l_{wg} < 3\lambda$ to avoid reflections and kill spurious modes. The height of the rectangular waveguides was chosen to be the same as for the resonant cavity, like in [18].

The centre port is positioned in the centre as that is a point where the resonant mode has a maximum for all signals inserted in the combiner, which applies for all radial combiner and divider structures. The centre port waveguide is chosen to be circular to simplify coupling between the TM_{0m0} mode in the cavity and the TM_{01} mode in the output waveguide.

The peripheral ports are uniformly distributed around the cavity side walls in order to excite a circularly symmetric mode, such as TM_{0m0} [18]. The number of peripheral ports depends on the need of amplification, as one peripheral port is used for every SSPA. The number of ports is an important design parameter as it affects the Q-factor of the resonator, which in turn is related to the bandwidth. The resonant mode is also chosen with consideration to the number of ports [9]. Last but not least, it is not physically possible to combine any number of input ports in a circular cavity as there simply is not room enough around it. In order to study the effect of different number of ports, three versions of the conceptual structure was used: a 4-port, a 6-port and an 8-port combiner or divider structure (displayed in Figure 3-4). Studies on how to include more ports on the cavity walls by for example multiple waveguides along the height dimension could be interesting in further work.

a)   b)   c)
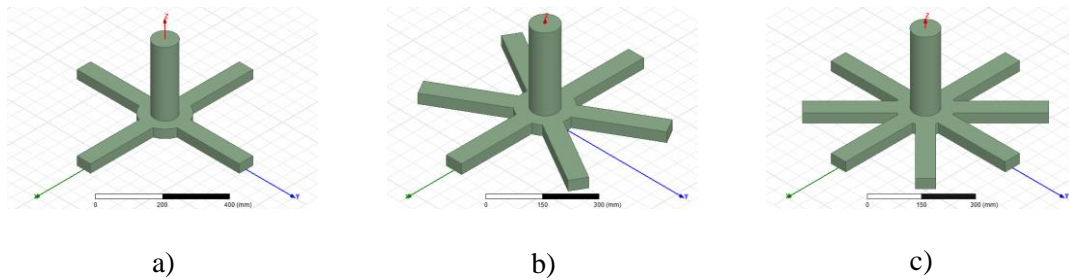
Figure 3-4. Three conceptual cavity combiner designs with waveguide ports: a) 4-port cavity structure, b) 6-port cavity structure and c) 8-port cavity structure.

In section 2.1, the equivalent circuit model for a resonant cavity was introduced. It can be a useful tool to understand the system in its completeness, when circuit models of the ports are added to it. Figure 3-5 shows the equivalent circuit for an *N*-port cavity combiner. As losses should be prevented in the system and the bandwidth is important, impedance matching is a large part of the design of a cylindrical cavity combiner or divider.
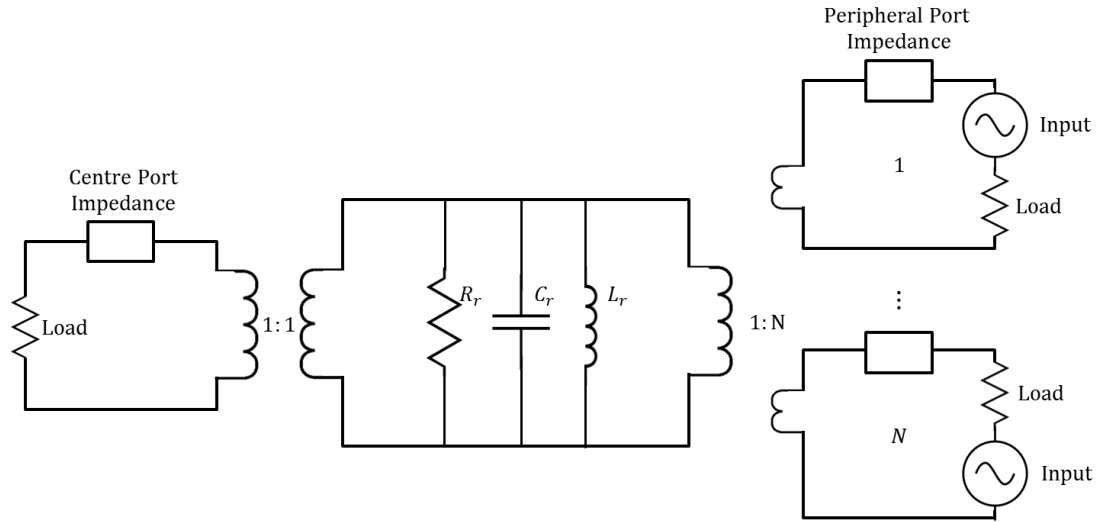
Figure 3-5. Equivalent circuit of an *N*-port combiner structure.

3.1.3 Impedance Matching

For waveguide junctions, mechanical modifications of the waveguides can be used to adjust impedance, and by that reduce reflection losses. Montgomery, Dicke and Purcell [5] describe how thin metal sheets can be inserted in waveguides to introduce a shunt reactive element jB, when the thin metal sheets form a slit through which the electromagnetic field can propagate. The detailed expressions for this are listed in APPENDIX C. The orientation of the slit opening determines if the reactive element is inductive or capacitive; a slit parallel with the electrical field will give rise to a shunt inductance, while a slit perpendicular to the electrical field will give rise to capacitive impedance [5]. For circular waveguides, no data is found for the TM_{0m} modes. It is, however, stated that for circular waveguides supporting TE_{11} modes, that addition of a metal sheet creating an iris opening gives rise to a shunt inductive susceptance [5].

Three different modifications of the waveguides in the 4-port structure was tested and analysed: addition of 7 mm high horizontal slabs to the peripheral waveguides, addition of an aperture iris rim of 9 mm at the circular, centred waveguide and finally, the radial position of the peripheral waveguides was shifted outwards so that the walls of the rectangular waveguides acted as 6.75 mm vertical slabs (as done in [18]). The modifications are shown in Figure 3-6 and Figure 3-7 below. Figure 3-9 and Figure 3-10 show simulated results of addition of metallic obstacles in the waveguide aperture junctions. The ports in the designs are numbered as in Figure 3-8.
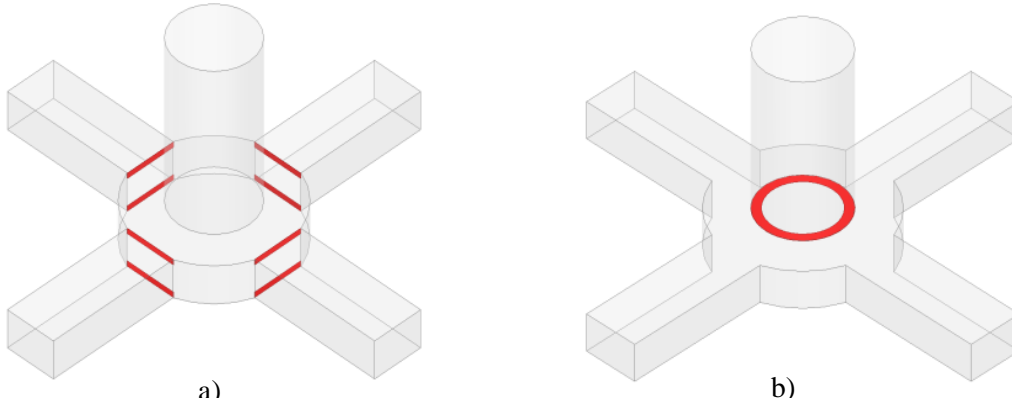
Figure 3-6. Addition of metallic obstacles (red) to the 4-port design; a) horizontal slabs and c) output aperture iris.
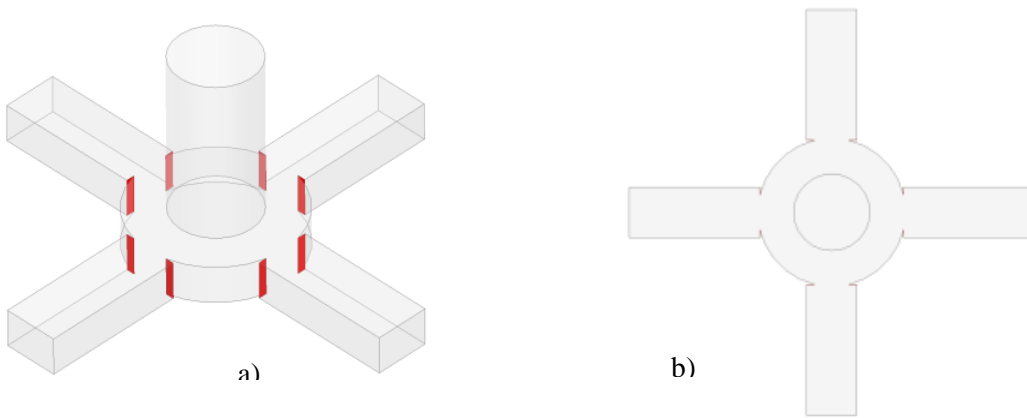
Figure 3-7. An outward shift of the peripheral waveguides in the radial direction creates a metallic obstacle (red) in the junction between the cavity and the waveguides.
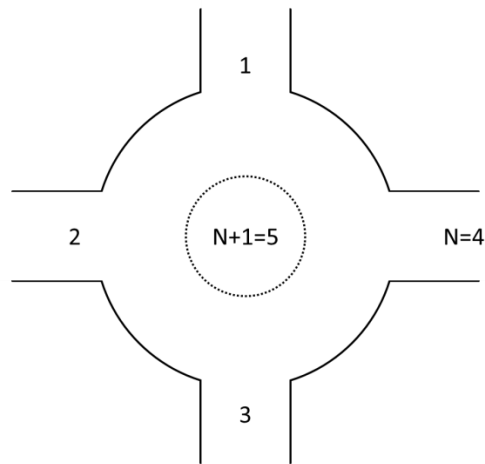
Figure 3-8. The peripheral ports are numbered 1 to N (counter clockwise), and the centre port is numbered $N+1$.

From Figure 3-9, it is clear that addition of a vertical slab will reduce reflections at the peripheral ports, while it increases reflections at the centre port. On the other hand, addition of

a horizontal slab will have the opposite effect and increase reflections at the peripheral ports, while reducing reflections at the centre port. The coupling factor that ideally should be

$$S_{15} = S_{51} = 10 \log_{10} \left(\frac{1}{5-1} \right) = -6.02 \text{ dB} \qquad (3.2)$$

is also changed with the addition of metallic sheets.

Figure 3-10 shows how the scattering parameters change when a thin, circular metal frame is added as an aperture iris. The reflection at the peripheral ports is reduced while the reflection at the centre port is increased. The coupling between central and peripheral ports is also reduced. This, however, does not mean that there always will be a trade-off between peripheral port matching and the other parameters; many other variables in a system can be varied, such as the cavity height and choice of ports. Depending on what type of port that is chosen for a combiner structure, ways to change the impedance must be determined. By knowing how the modifications of the port affects the network, equivalent circuit models can be used together with the network for the resonator in software such as Keysight ADS or Microwave Office, where optimizations can be performed that predicts what kind of modifications that need to be used for the ports.
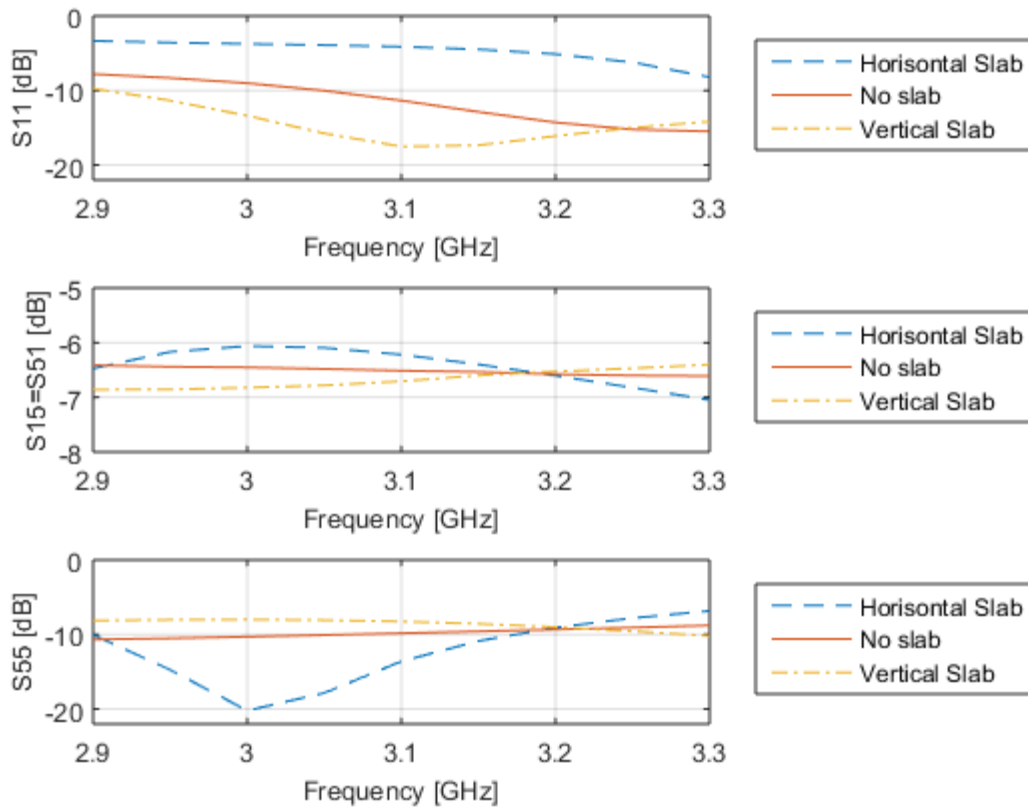
Figure 3-9. Simulated effect of impedance alternation performed with slits and diaphragms in the aperture junction between the cylindrical cavity and the peripheral rectangular waveguides for the 4-port structure.
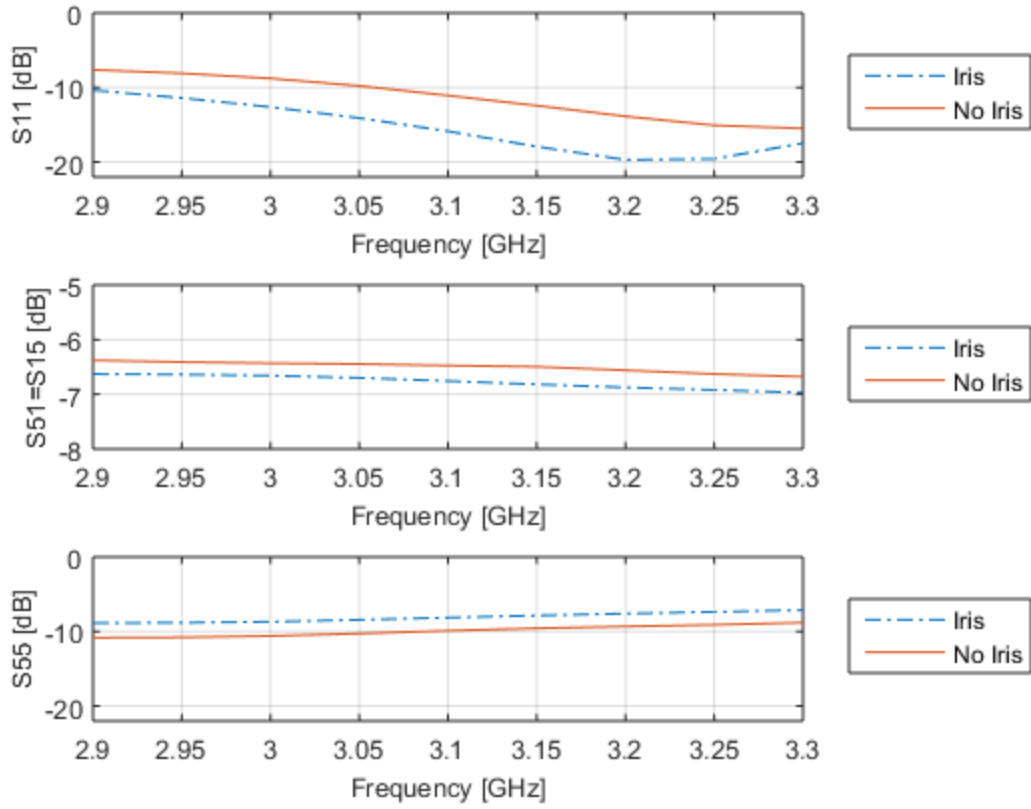
Figure 3-10. Simulated effect of impedance alternation performed with aperture iris in the aperture junction between the cylindrical cavity and the centred circular waveguide for the 4-port structure.

All scattering parameters in the scattering matrix are related (as discussed in section 2.1.4) and matching at one port will affect the matching at all other ports. This is where the equivalent circuit in Figure 3-5 is a useful tool when the whole system is considered. The peripheral ports are connected in parallel and can be lumped together to one total input impedance $Z_{peripheral}$ seen from the resonant cavity

$$\frac{1}{Z_{peripheral}} = \frac{1}{Z_{\mathrm{wg}}} + \frac{1}{Z_{wg}} + \cdots = \frac{N}{Z_{wg}} \rightarrow Z_{\mathrm{peripheral}} = \frac{Z_{\mathrm{wg}}}{N}. \tag{3.3}$$

This means that there will be at least two steps in impedance in the structure that need to be matched: the junction between the cavity and the centre port and the junction between the cavity and the peripheral ports.

Addition of an impedance modification as any shunt reactance to the equivalent circuit will obviously change the resonant frequency of the resonator. This is not necessarily a problem as the cavity can be adjusted accordingly. Another cause of worry is what happens when the thin metallic sheets are exposed to high power electromagnetic fields and surface currents are induced. This is not investigated within this project, but could be interesting to study further.

3.1.4 Bandwidth

The narrow bandwidth of cylindrical cavity resonators has already been discussed in previous chapters as well as the fact that addition of ports decreases the Q-factor, hence broaden the bandwidth [9]. In order to make an accurate comparison between the bandwidth of the three different concept structures (the 4-port, the 6-port and the 8-port), all three structures should first be optimized individually as the load from the peripheral ports will vary seen from the resonator. This was however not done in the scope of this master thesis project.

The bandwidth can be estimated with a mathematical approach, by using the equivalent circuit model and study the coupling between the ports and the resonators. The bandwidth is found by calculation of the loaded Q-factor, Q_e, that is related to the coupling factor and the unloaded Q-factor of the resonator.

3.1.5 Isolation

For cylindrical cavity combiners and dividers, leakage between the peripheral ports is a result of resonance of spurious modes within the cavity [18]. For the concept structure, no mode suppression is used which means that the leakage shown in Figure 3-11 is a worst case scenario. Figure 3-11 shows the leakage between input ports for all modes that resonates when the cavity is excited by TE_{10} modes in the peripheral waveguides. The mean leakage gives an idea of how much inserted power will be lost through other input ports.
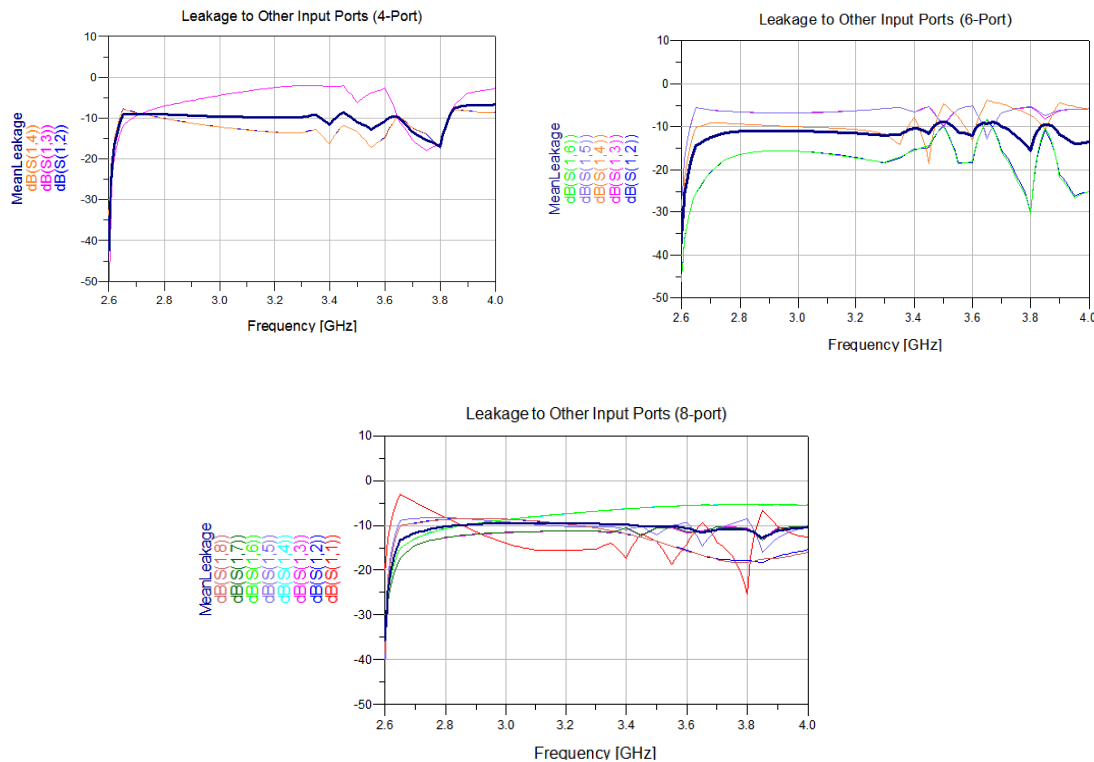
Figure 3-11. Simulated leakage shows the isolation between input ports for all modes excited by TE_{10} modes in the peripheral waveguides. The mean leakage between ports is marked with a thick dark-blue line and is at 3.1 GHz: -9.746 dB for the 4-port, -11.213 dB at the 6-port and -9.547 dB for the 8-port structure.

For better isolation, spurious modes should be identified and suppressed as far as possible. It is however worth to remember that perfect isolation and perfect port matching and coupling cannot be achieved simultaneously.

3.2 Design Requirements for Prototype Divider and Combiner

One of the aims of this project was to design and fabricate a prototype divider and combiner with excellent performance, and to determine its usability in a SSPA based amplifier solution for radar applications. A literature study was performed where properties of different dividers and combiners were compared and listed in tables in section 2.3.1-2.3.3. The goal was to achieve insertion and reflection loss as good as, or better than, similar published designs.

An important factor in the choice of technology was of course the feasibility of the fabrication, as the project was limited by both time and funds.

3.2.1 Amplifier

The design was initially planned to be used together with an amplifier that operates between 2.9 GHz and 3.3 GHz, and the design is therefore optimized for these frequencies. However, due to practicalities, the amplifier in the actual test setup was replaced with InGaP HBT amplifiers that operate at DC-4 GHz with a listed typical gain of 11.7 dB and a P_{1dB} of 17.3 dBm [29]. All eight amplifiers were measured and the variation in gain and phase between the individual amplifiers were so small that they were considered to be identical.

3.2.2 Central and Peripheral Ports

Radar requires large output powers as the range of the radar is related to the transmit power as $R \propto \sqrt[4]{P_{transmit}}$ [30]. For military radar, the output power levels are often of the order of several kW, hence, the combiner and its output must be able to handle such power levels. In a real life application, it is likely necessary for the combiner to have a waveguide output, as they are able to handle very high powers safely. The initial design idea was therefore to use a waveguide output for the prototype combiner as well. That was, however, changed during the design process due to time limitations and coaxial contacts were used as input and output ports for both the divider and combiner, which is discussed in section 3.3.2.

3.2.3 Number of Ports

Another consequence of the high output power required is that a high number of amplifiers must be used, as the performance of SSPAs is still limited to hundreds of Watts. As many ports as 50-100 might be needed in real life applications. In order to reduce the complexity of the design, it was decided that the prototype should have eight input ports. This is a major limitation in this study, as the number of ports is an important aspect to consider in choice of technology, and also affects the characteristics of the combiner design.

3.2.4 Bandwidth

The bandwidth of the combiner and divider was set to be the same as for the amplifier that was initially supposed to be used in the test setup: 2.9 GHz-3.3 GHz. This results in a bandwidth of 13 %.

3.2.5 Isolation

In the ideal case, the peripheral ports should be completely isolated from each other. Different realization methods of combiners and dividers allow different level of isolation. For this project, as good isolation as possible was strived for but not deemed a crucial requirement in the choice of design.

3.3 8-port Cylindrical Cavity Divider and Combiner Prototype

This section describes the design process of the cylindrical cavity divider and combiner prototype. A passive structure was designed according to the design requirements discussed in 3.2, and the structure was to be fabricated in two identical copies; one of them to be used as a divider and the other one to be used as a combiner.

The prototype is an 8-port TM_{020} cylindrical cavity structure with SMA-connectors as centre and peripheral ports.

3.3.1 Design of Cylindrical Cavity

The cylindrical cavity was designed as described in 3.1.1; the radius was calculated from (2.4) – the expression for cutoff frequencies – for the TM_{020} mode and the height was initially left undetermined as it is one of the tunings parameters used for impedance matching. The cavity was modelled in HFSS as a vacuum cylinder with arbitrary height $d < \lambda/2$.
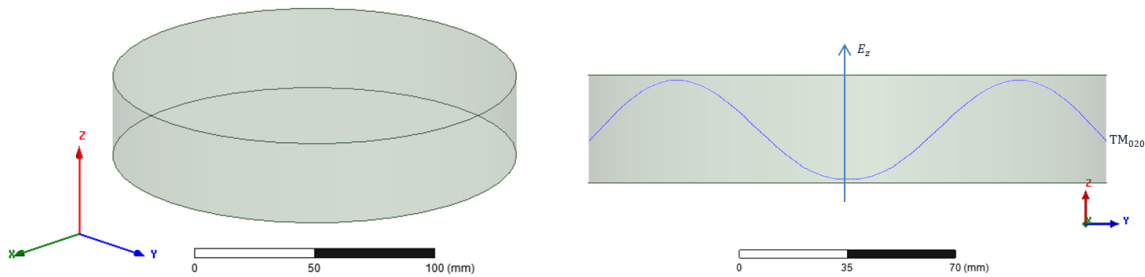
Figure 3-12. The cylindrical cavity model in HFSS, with the field function for the E_z field of the TM_{020} mode drawn on top of it.

3.3.2 Peripheral and Centre Ports

50 Ω SMA-connectors with long coaxial probe pins were used for the peripheral and centre ports, and were modelled in HFSS using data from the datasheet [31]. The centre pin of the coaxial connector is used as a probe to excite the resonant cavity for the input ports; for the output ports the reversed process takes place, and the probe is excited by the fields in the cavity.
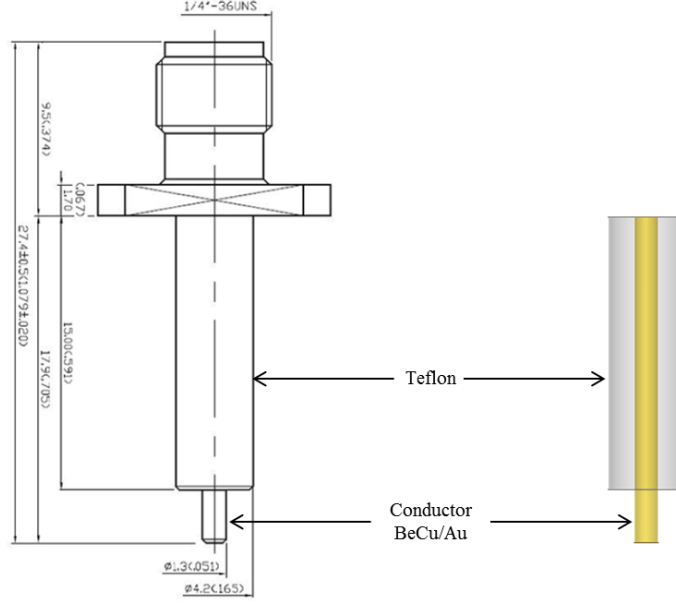
Figure 3-13. **Left:** Sketch of the SMA-connector according to data from the datasheet [31].
Right: Model of the SMA-connector made in HFSS.

To optimize power transfer and excite the correct mode, the peripheral ports should be located at the radial distance ρ where E_z has a maximum [9]. The field expression for E_z is taken from Table 2-1, and the field maximum can be found from

$$\frac{\partial}{\partial \rho}(A \sin n\emptyset + B \cos n\emptyset)J_n(k_c\rho)e^{-j\beta z} = 0. \qquad (3.4)$$

It is clear from the expression that only the Bessel function is dependent on ρ, and the equation can be simplified to

$$J_n'(k_c\rho) = 0 \qquad (3.5)$$

and so, the solution $p_{nm}' = k_c\rho$ for $nm = 02$ can be found from Table 2-2. The calculated radial distance $\rho = 59.2$ mm was used as a starting point for optimizations in HFSS. After optimizations, the final radial distance was set to $\rho = 62.04$ mm. Figure 3-14 shows the E-field in the cavity when the ports are positioned as described and the centre positioned input port is excited. Below the resonator, the E_z-field for the TM_{020} mode is plotted to show the positions of the theoretical maxima.

E Field [V/m]

7.8153E+03
7.0339E+03
6.5651E+03
6.0962E+03
5.6274E+03
5.1586E+03
4.6897E+03
4.2209E+03
3.7521E+03
3.2832E+03
2.8144E+03
2.3456E+03
1.8767E+03
1.4079E+03
9.3907E+02
4.7024E+02
1.4022E+00

TM_{020} mode in resonator
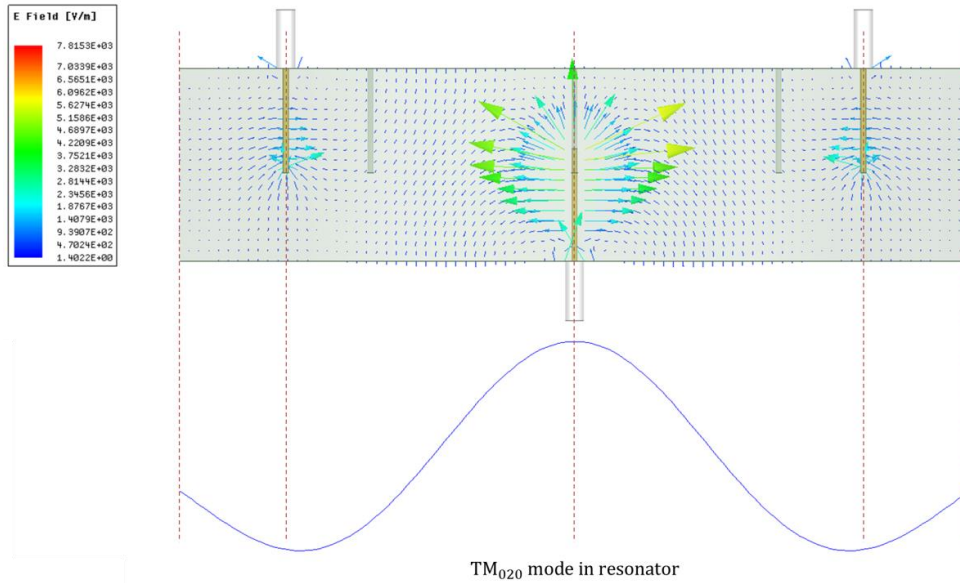
Figure 3-14. Cross-section of the resonant cavity with the E_z-field component of the TM_{020} shown. The probe is inserted in the region of a maximum of the field to optimize power transfer.

Initially, the combiner was planned to have a rectangular waveguide output, as would probably be the case in a real life radar application, and a number of output waveguides and transducers were tested. None of them resulted in sufficient impedance matching and the waveguide output was therefore replaced with a SMA-connector which led to identical designs for the divider and combiner. The interested reader finds the tested solutions with the simulation results in APPENDIX A . How a rectangular output is implemented in the best way is an interesting topic for further work.

3.3.3 Impedance Matching by Connector Modification

The prototype has identical peripheral and central output ports, which caused impedance mismatch as the peripheral ports are equivalent to parallel loads, as discussed in 3.1.3. For a good matching, the peripheral and centre port should both be matched to the cavity impedance. However, the impedance for the peripheral ports should be around N times as high as the impedance for the centre port. Hence, the centre and peripheral ports should have different impedance and that was to be accomplished by modification of the coaxial probes.

The easiest way to change the impedance by modification of the SMA connectors would be to cut of the centre pins to different lengths, but this did not result in a good enough result. Instead, copper cylinders with variable dimensions were added to the conductor pins in the coaxial connector. All peripheral ports were set to be identical since circular symmetry should apply to the design, which leaves three impedance parameters: impedance of peripheral ports, impedance of the centre port and impedance of the cavity, where the latter is varied by variation of the cavity height.

To study the effect of the copper cylinder modifications, a simulated model of the resonant cavity was set up where the peripheral connectors were unmodified. The centre connector had a copper cylinder attached to the connector probe, as displayed in Figure 3-15 and the following three dimensions were varied: the cylinder height, the cylinder radius and the cylinder position. The parameter study does not give a full understanding of how the probes

30

should be modified for optimal performance, but should give a sense of how sensitive the dimensions of the probe are for alternation.
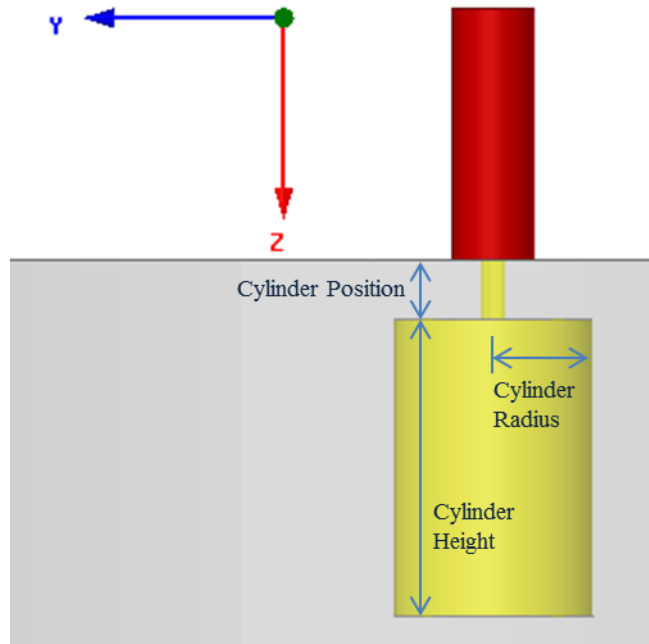
Figure 3-15. Modified coaxial pin with added copper cylinder with three variable dimensions that affect impedance: the cylinder height, cylinder radius and cylinder position.

The effect on the scattering parameters of the combiner impedance of the ports varies as in Figure 3-16, Figure 3-17 and Figure 3-18. It is clear that small changes in the dimensions and position of the cylinder have a large impact on the impedance matching at the ports and the coupling between the centre and peripheral ports. The copper cylinder's dimensions are therefore very suitable as tuning parameters in an optimization where the copper cylinder at the centre port and the copper cylinders and the peripheral ports can be varied simultaneously, in order to design the structure for optimum performance.
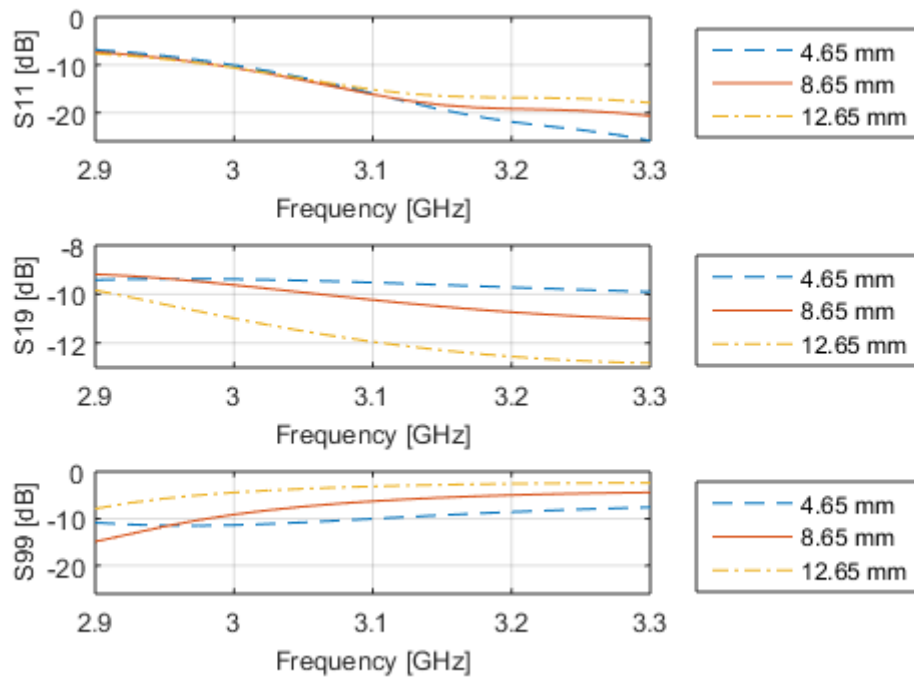
Figure 3-16. Simulated results of variation of the radius of copper cylinders used for modification of connector probes.
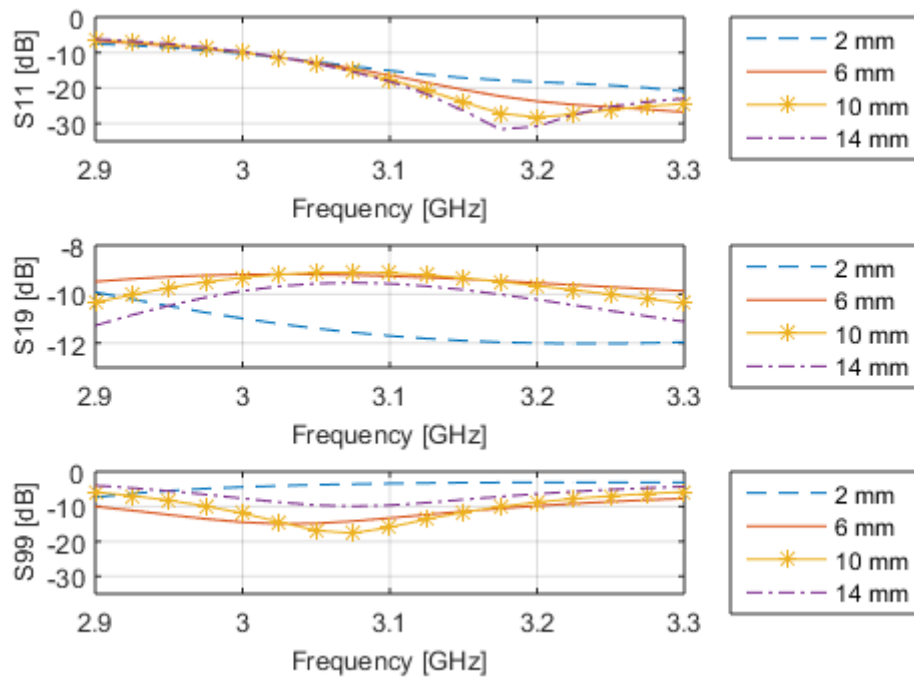
Figure 3-17. Simulated results of variation of the position of copper cylinders used for modification of connector probes.
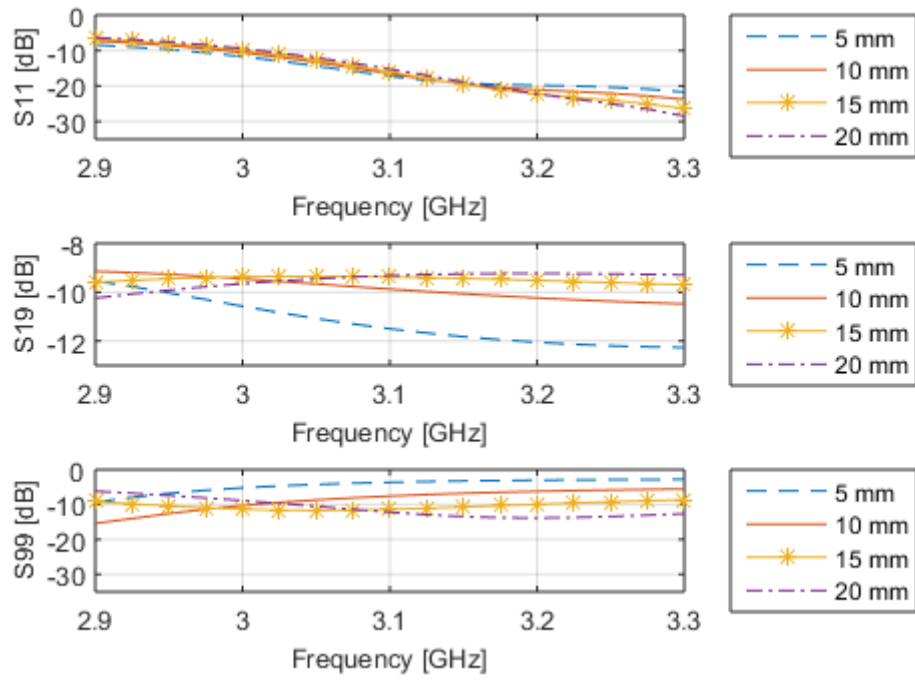
Figure 3-18. Simulated results of variation of the height of copper cylinders used for modification of connector probes.

The whole structure was optimized with the following variables seven: cavity height, peripheral port cylinder height, peripheral port cylinder radius, peripheral port cylinder position, and centre port cylinder height, centre port cylinder radius and centre port cylinder position. An optimization with extra weight on the reflection coefficients at the ports led to the design seen in Figure 3-19 and the scattering parameters in Figure 3-21. The E-field of the design is displayed in Figure 3-20.
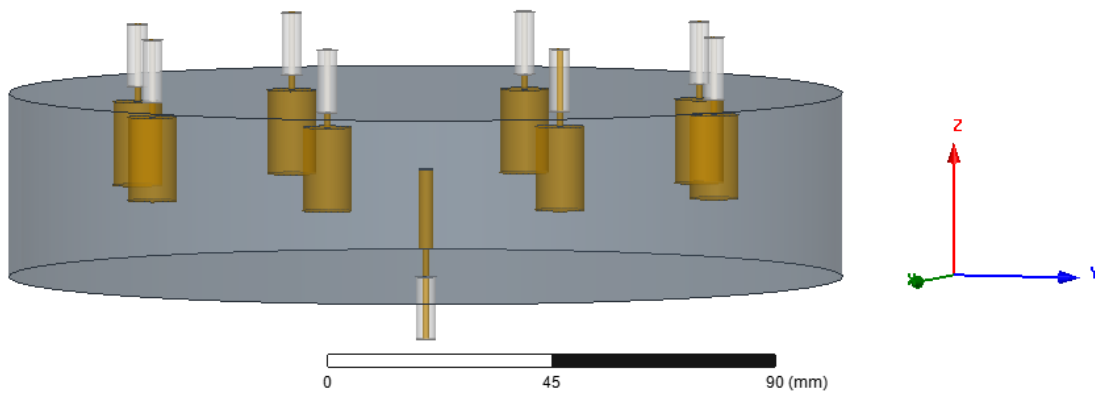
Figure 3-19. Optimized design of the cylindrical cavity divider and combiner.
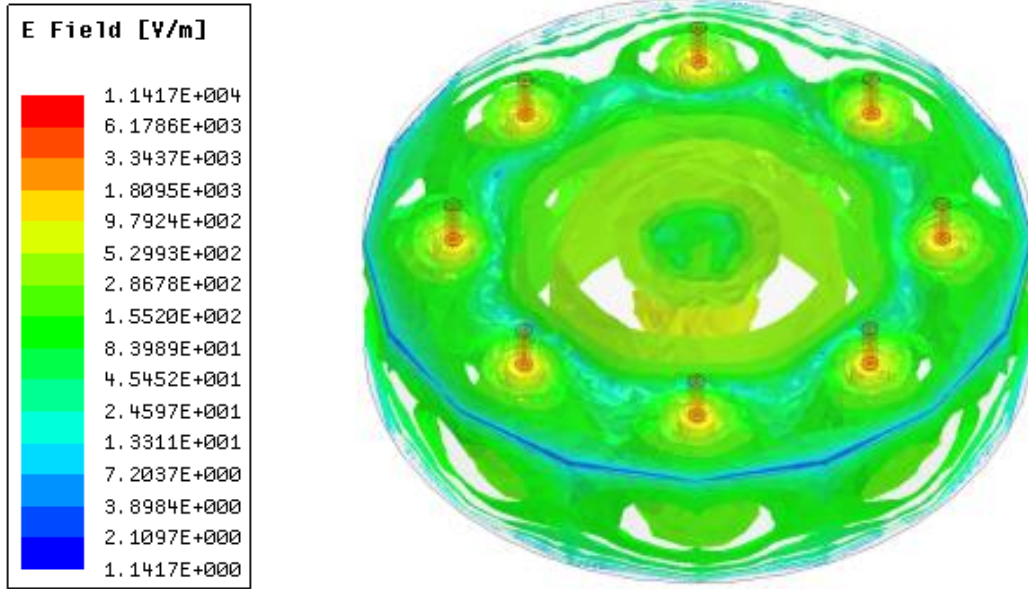
Figure 3-20. E-field in the optimized structure when the centre port is excited with 1 W.

The simulated values for the design gives a centre port return loss better than 16.6 dB for 2.9 GHz-3.3 GHz, and a peripheral port return loss better than 15.0 dB. The insertion loss is better than 0.1 dB for 2.9 GHz-3.3 GHz and is identical for the combiner and divider case as the design is reciprocal.
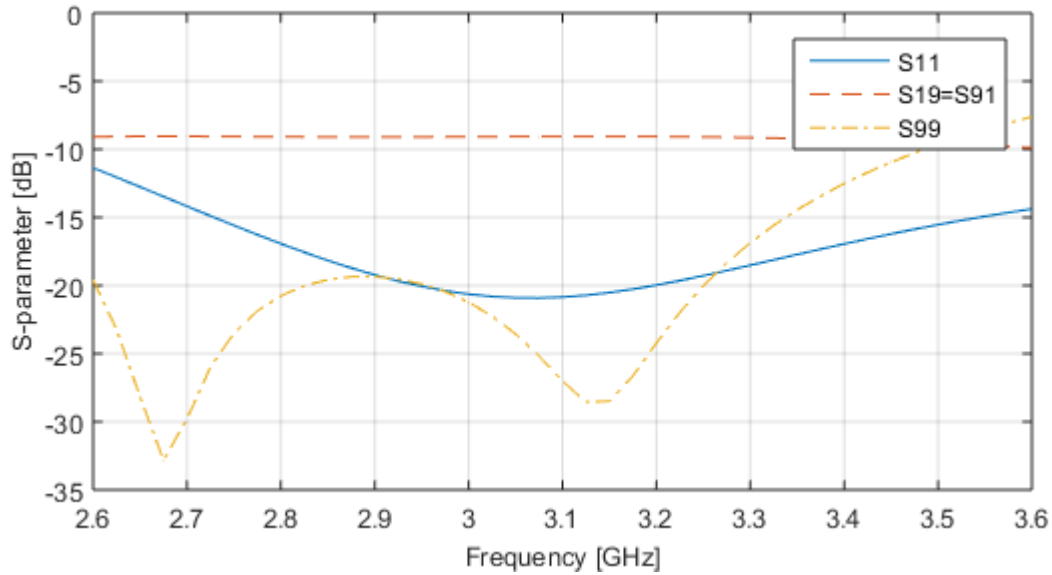
Figure 3-21. Scattering parameters of the optimized design of the structure.

3.3.4 Measurements of Final Design

The design with copper cylinders was optimized for maximum input matching which resulted in the design displayed in Figure 3-19. The measurements for the design are listed in

Table 3-1. Final measurements of the optimized design.

Design Parameter	Value [mm]
a_{res}	85.00
d_{res}	37.44
h_1	17.02
h_2	16.20
r_1	5.00
r_2	1.50
z_1	3.06
z_2	5.70
ρ_{port}	62.04
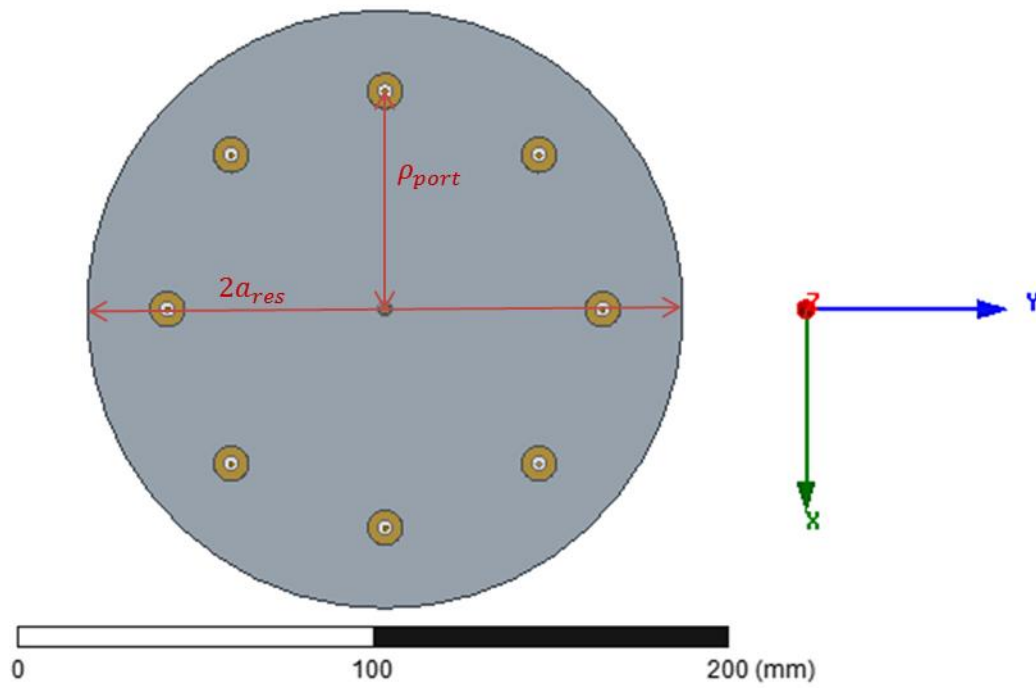
Figure 3-22. The final design from above.
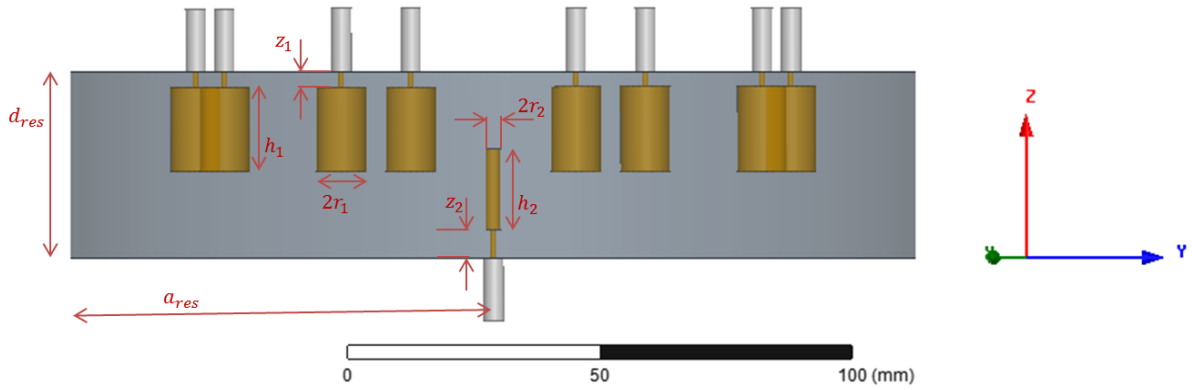
Figure 3-23. Cross-section of the final design.

3.4 Fabrication of Prototype and Test Setup

The test setup used to measure the performance of the structure consists of one divider, eight amplifiers and one combiner. This section will cover the fabrication of the divider and combiner structure, which have the same design, and what practicalities need to be taken into consideration to create a physical prototype as similar to the simulated model as possible.

3.4.1 Fabrication Considerations of Divider and Combiner

The cavity in the divider and combiner structure is milled from aluminium, with a tolerance in the height dimension of ±0.2 mm. The cavity was created by two aluminium pieces joined together with screws, as seen in Figure 3-24.
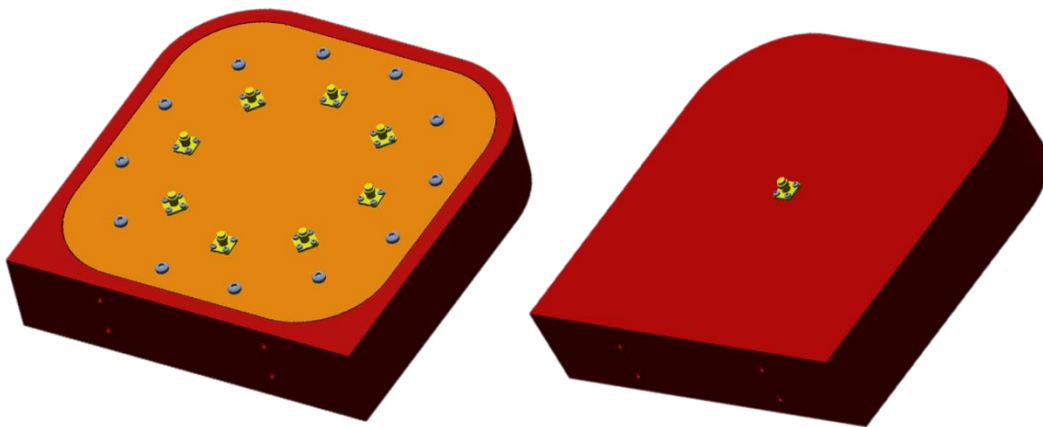
Figure 3-24. The fabricated structures with the peripheral ports on the lid (orange) of the box to the left and the centre port at the bottom of the box (red) to the right. The SMA connectors (yellow) and screws that close the box (grey) are also seen.

The joint between the aluminium part containing the cavity and the aluminium lid that closes the cavity was positioned where the conducting surface surrounding the cavity has low surface currents. This choice was made to minimize disturbance of the field within the cavity and to prevent electrical leakage.

Figure 3-25 shows the surface currents on the cylindrical cavity. With regard to this and practical aspects in the assembling of the test setup, a design where the cylindrical cavity is milled in a piece of aluminium and closed with an aluminium lid that was screwed onto the cavity was chosen.
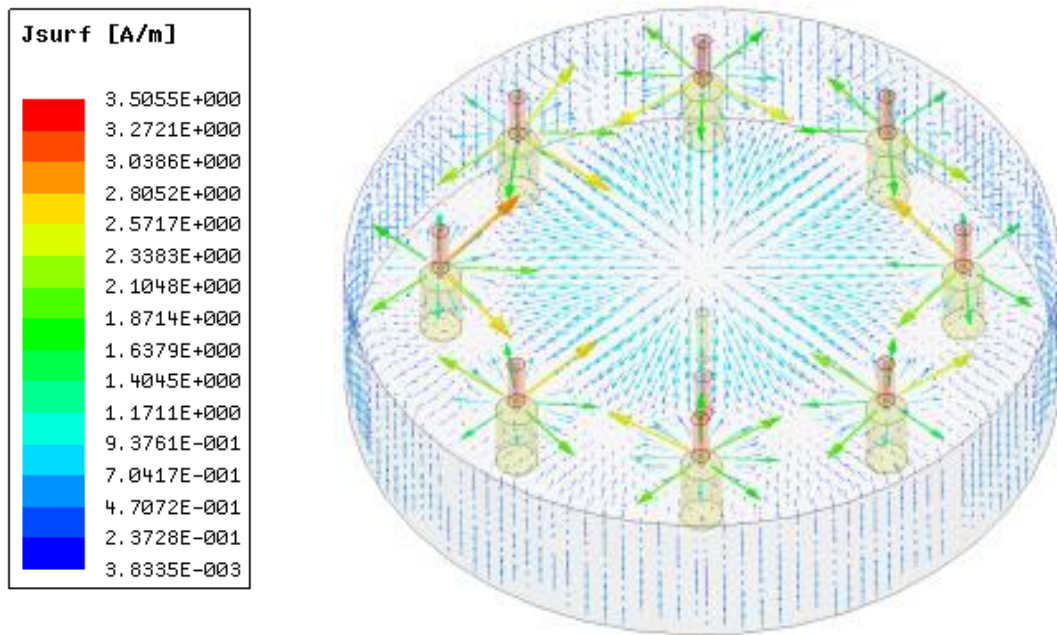
Figure 3-25. Surface currents plotted on the cylindrical cavity. The upper corner is of special interest as it is the place for the junction in the fabricated prototype.

The metallic, cylindrical box and the lid are shown in Figure 3-26. To prevent radiation to leak from the cavity, the gap around the lid is shifted a few mm from the cavity walls, as seen in Figure 3-26. This prevents radiation leakage in the event of a un-tight lid.
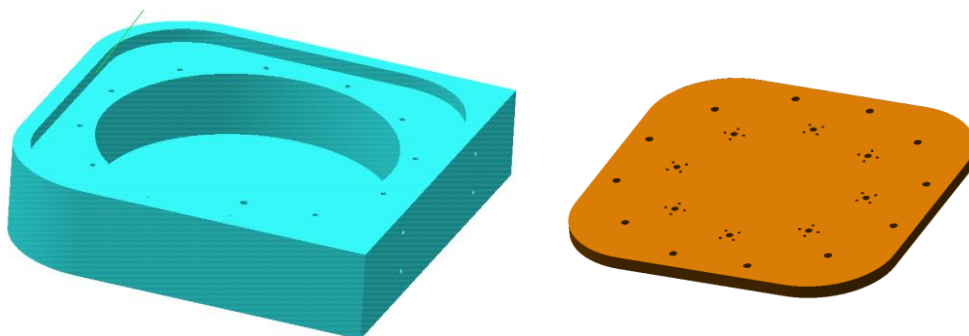
Figure 3-26. The cylindrical cavity box and the lid, both in aluminium, surrounding the cavity that the divider and combiner are based on.

3.4.2 Fabrication of SMA Connector Probe Modifications

The SMA connectors were purchased with a standard radius and length of the coaxial centre pin, and custom made copper cylinders were designed to be soldered onto the pins by hand. Each cylinder has a drilled hole with a certain depth to help fixate the cylinder at the correct distance from the cavity lid, to simplify the soldering. An air valve at the bottom of the hole is also added to make it easier to get the solder into the hole.

The size of the copper cylinder in combination with the manual assembly of the probe modifications complicates the fabrication, and it is hard to predict the uncertainties. In Figure 3-27, the measurements and tolerances of the probe modifications are displayed. The outer measurements are also found in Table 3-1 on page 35.
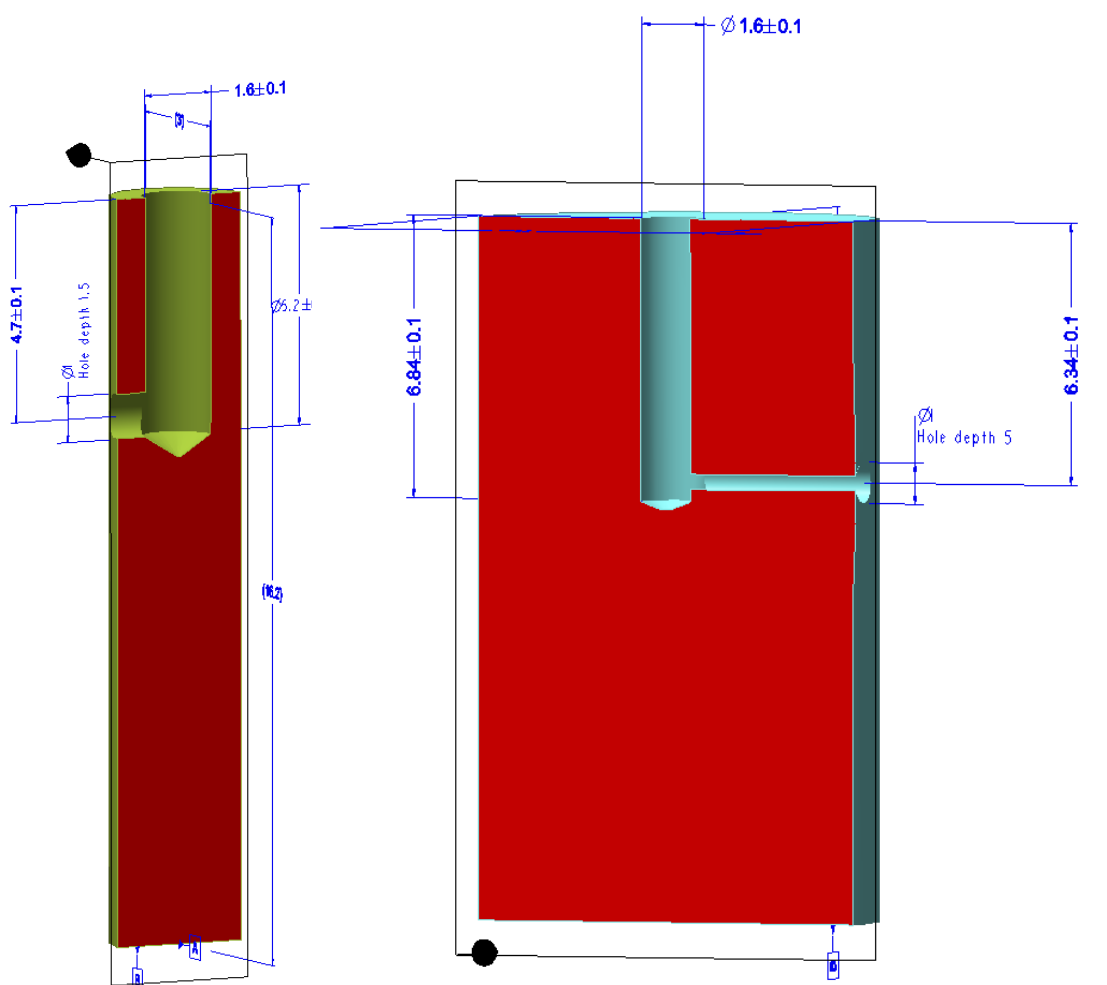
Figure 3-27. Measurements and tolerances of the copper cylinders used for probe modification. The left cylinder is the centre port modification to the connectors at port 1-8 and the right cylinder is the peripheral port modification to the connector at port 9.

4 SIMULATED AND MEASURED PERFORMANCE

In this section, the performance of the designed divider/combiner structure is evaluated and the measured results from the two fabricated prototypes are compared to the simulated results. The fabricated structures are evaluated as both dividers and combiners, since they should be passive and identical to each other. They will be referred to as structure 1 and structure 2. In test setups where they are connected to each other to create a two port system, structure 1 divides the signal and structure 2 recombines it.

The simulations are all based on the structure that was designed and optimized in HFSS. The scattering matrix from the optimized design is imported into networks in ADS for some simulations. The simulations in ADS do in general not include devices as connector adapters and such, which can lead to differences in measured and simulated results.

4.1 Comparison of the Fabricated Structures and the Simulated Model

First, a comparison between the assembled divider/combiner prototypes and the simulated results was made. Since the copper cylinders from section 3.3.3 were soldered to the SMA connectors by hand, the behaviour of all peripheral ports was measured to evaluate the symmetry of the prototypes. The forward port of a 2-port VNA was connected to a peripheral port (port i) at the structure, and the reverse port was attached to the centre port (port 9). With this procedure, eight measurements – one for each peripheral port – was performed.

4.1.1 Scattering parameters

The resulting scattering parameters from the measurements are displayed in Figure 4-1 and Figure 4-2. The corresponding scattering parameters for the simulated model are displayed in Figure 4-3, and are nearly perfectly symmetric. The variation is a result of the simulation method and the choice of mesh in HFSS. The measured reflection coefficient at the peripheral ports, S_{ii}, varies within a range of 5 dB for structure 1 and 12 dB for structure 2, which means that the structure is not very symmetric, which might affect the field in the cavity. The coupling $S_{i9} \approx S_{9i}$ should ideally be -9.03 dB but varies between -9.41 dB and -8.85 dB for structure 1 and -9.50 dB and -9.03 dB for structure 2 for the frequency band of 2.9 GHz to 3.3 GHz. This means that the division of power would not be symmetric for these structures. The reflection coefficient at the centre port S_{99} is measured in eight identical measurements – one for each measurement of the peripheral ports – and is -16.25 dB for structure 1 and -14.83 dB for structure 2.

A comparison of the performance of the measured structures and the simulated design is done in section 4.1.2 below.
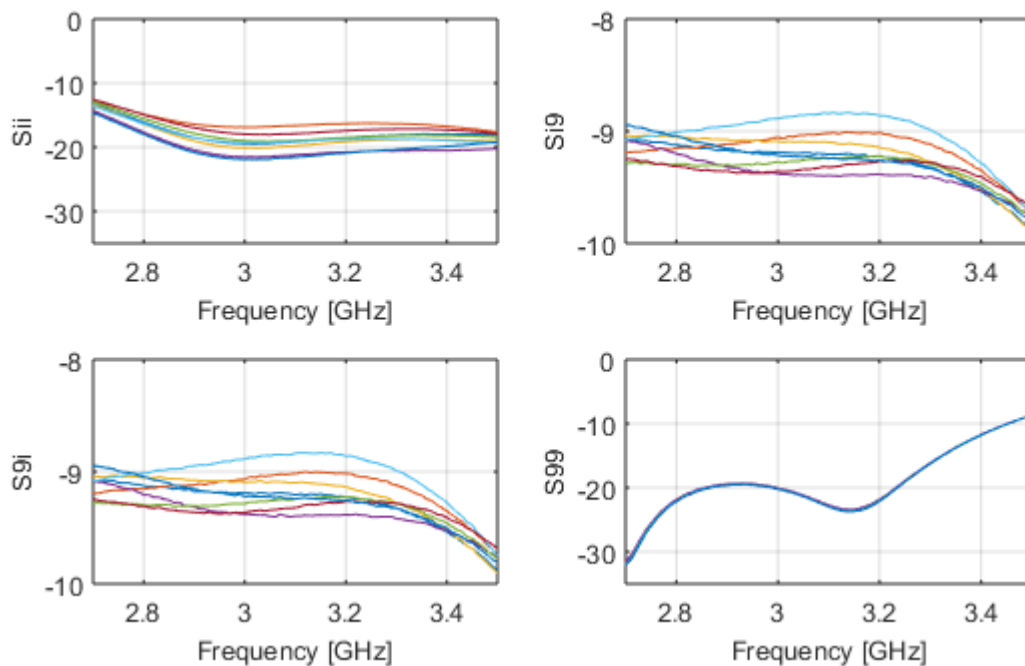
Figure 4-1. Measured scattering parameters of Structure 1. The reflection coefficient S_{ii} at the peripheral ports is less than -16.7 dB for all ports while the reflection coefficient at the centre port S_{99} is less than -16.3 dB for 2.9 GHz-3.3 GHz. The coupling parameters S_{21} and S_{12} varies between -9.4 dB and -8.4 dB.
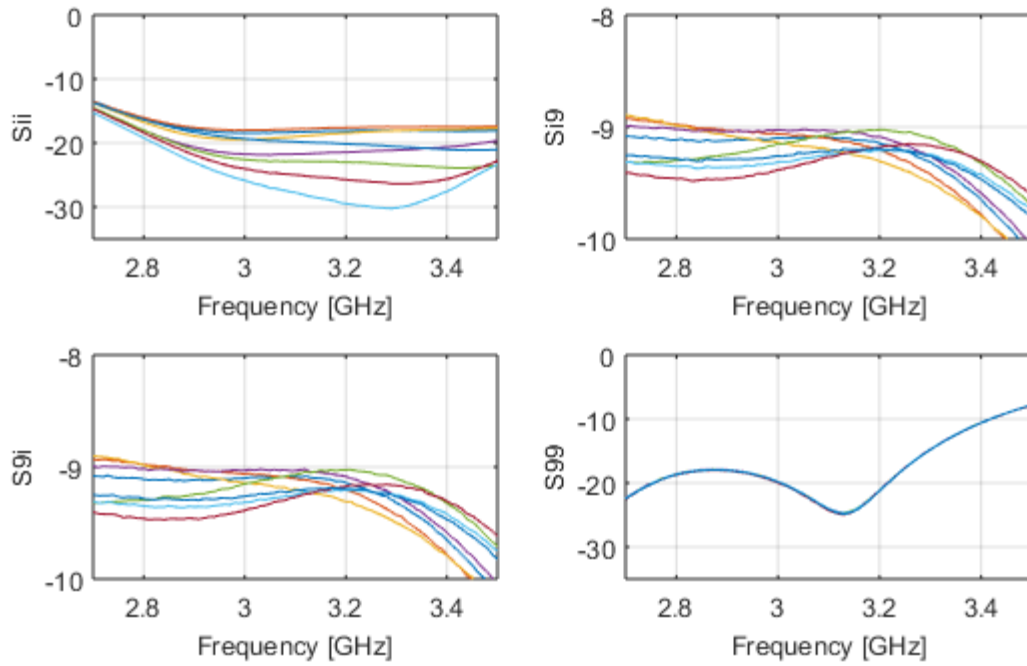
Figure 4-2. Measured scattering parameters of Structure 2. The reflection coefficient S_{ii} at the peripheral ports is less than -17.3 dB for all ports while the reflection coefficient at the centre port S_{99} is less than -14.8 dB for 2.9 GHz-3.3 GHz. The coupling parameters S_{21} and S_{12} varies between -9.4 dB and -9.24 dB.
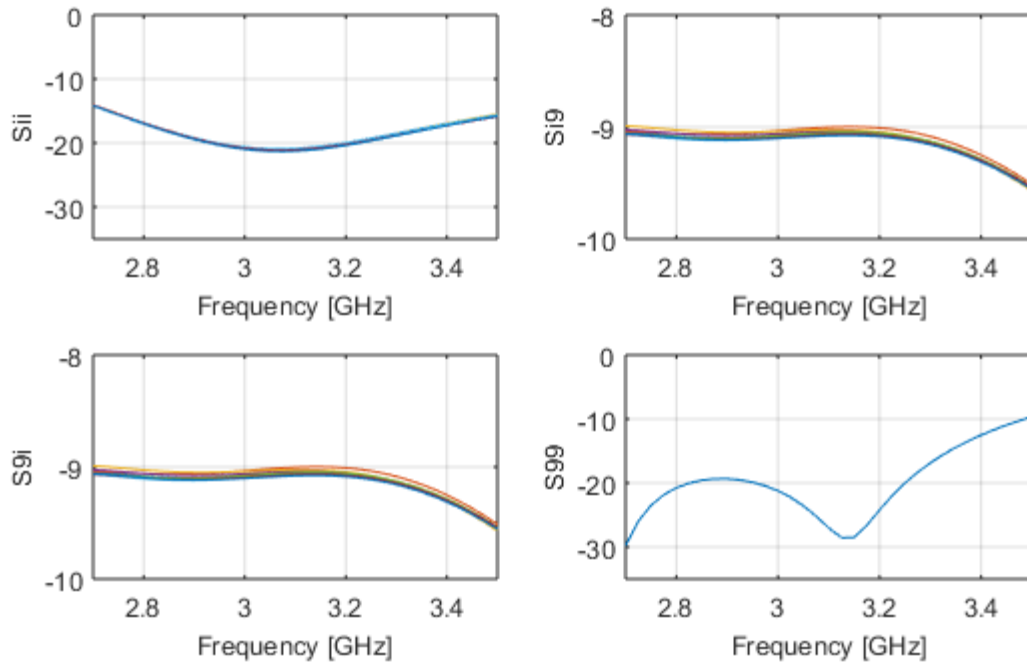
Figure 4-3. Simulated scattering parameters from the design process. The reflection coefficient S_{ii} at the peripheral ports is less than -19.1 dB for all ports while the reflection coefficient at the centre port S_{99} is less than -17.7 dB for 2.9 GHz-3.3 GHz. The coupling parameters S_{21} and S_{12} varies between -9.13 and -9.04 dB.

4.1.2 Return and Insertion Loss

The fabricated structures had identical designs which are passive and reciprocal, which means that they should be able to operate as both a divider and a combiner. The return loss (RL) and insertion loss (IL) was therefore calculated both when the peripheral ports acted as input ports and when the structure was excited at the centre port.

Figure 4-4 displays the return loss and insertion loss for the structures and the simulated model when they are used as combiners. That is, the return loss is calculated for each individual peripheral port from its S_{ii} parameter and the displayed value in Figure 4-4 is the average of the eight calculated return loss values. The measured return loss of the fabricated structures show a wider bandwidth than the return loss from the simulated model. The pass band is however shifted towards higher frequency, and has a centre frequency around 3.3 GHz, which is 0.2 GHz higher than the design frequency and means a shift in centre frequency of 6 %. Structure 1 has a RL=18 dB bandwidth of 0.8 GHz around 3.3 GHz which gives a bandwidth of 24 %. Structure 2 has a RL=19 dB bandwidth of 0.7 GHz around 3.2 GHz which gives a bandwidth of 21 %.

The insertion loss, however, is shifted by 6 % towards lower frequencies with centre frequency around 2.9 GHz, compared to design frequency of 3.1 GHz. Structure 1 has an IL= 0.20 dB bandwidth of 0.6 GHz around 2.9 GHz which gives a bandwidth of 22 %. Structure 2 has an IL=0.25 dB bandwidth of 0.7 GHz around 2.9 GHz which gives a bandwidth of 23 %.
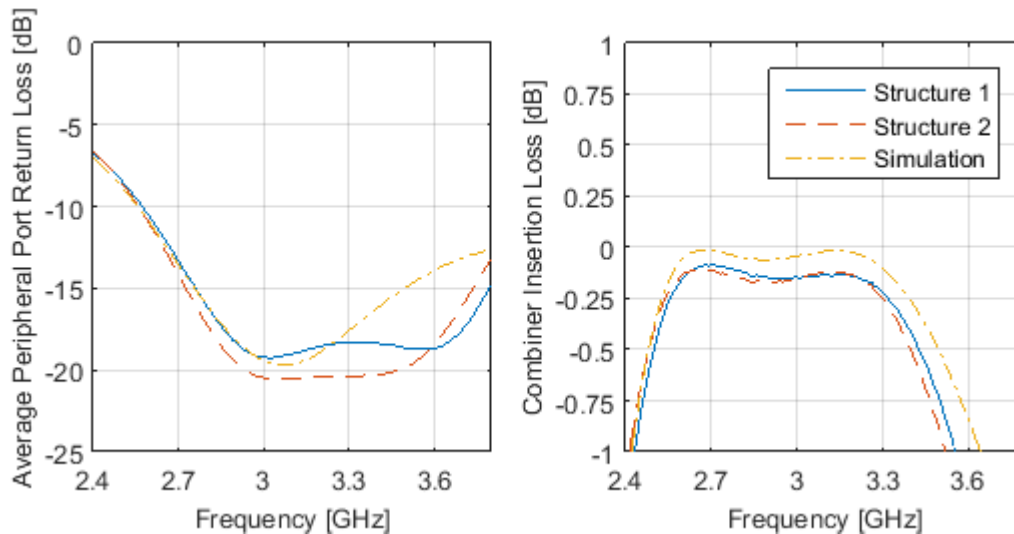
Figure 4-4. Average peripheral port return loss and insertion loss for the structures. The measured return loss of the structures shows a more broadband behaviour than the simulated values.

Figure 4-5 displays the return loss and insertion loss for when the structures and simulated model is used as a divider. The peaks in the return loss for the measurements follow the simulation well, while structure 1 shows slightly better performance in return loss for the lower design frequencies. Structure 1 has a RL=16 dB bandwidth of 0.7 GHz around 2.9 GHz which gives a bandwidth of 24 %.

A better RL performance can be achieved if the highest 0.05 GHz of the design frequencies are excluded from the design requirements; RL>19 dB is found for 2.61-3.25 GHz. Structure 2 has a RL=15 dB bandwidth of 0.7 GHz around 2.9 GHz which gives a bandwidth of 24 %.

As in the case with structure 2, a better RL can be achieved if the highest design frequencies are excluded from the passband; RL>17 dB for 2.60-3.25 GHz.

The insertion loss for the divider and combiner application should be identical according to theory and simulation. The measured result is consistent with theory.
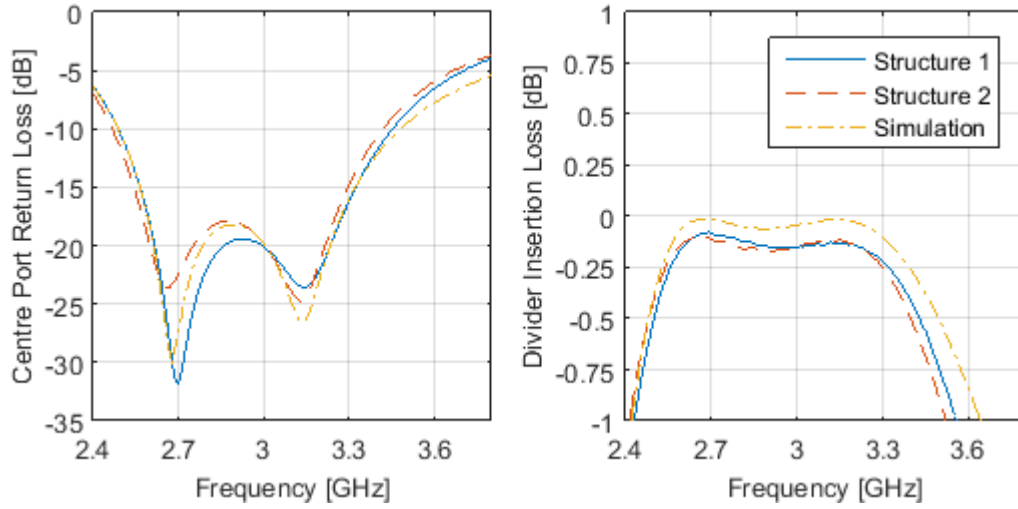
Figure 4-5. Centre port return loss and insertion loss for the structures. The simulated result show smaller insertion loss than the measurement, while the measured centre port return loss behaviour is very similar to the simulation.

4.1.3 Leakage and Isolation

For the measurement of isolation between peripheral ports, a peripheral port of each structure was chosen as reference, called port 1. The ports with the behaviour closest to average behaviour were chosen, and the remaining peripheral ports were numbered as in Figure 4-6.
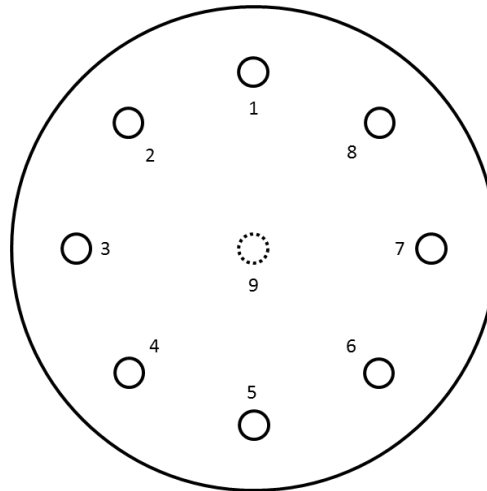
Figure 4-6. Numbering of the peripheral ports, ports 1-8. The centre port on the opposite side of the cavity is port number 9.

The measured leakage between port 1 and the other peripheral ports for structure 1 and structure 2 is displayed in Figure 4-7 together with the simulated values. From the simulated values, it is seen that port 1 couples strongest with its opposite port, port 5, and the neighbour

43

ports, port 2 and 8, which was confirmed in the measurements. Only port 4 and port 6 show better isolation than 10 dB for 2.9 GHz-3.3 GHz, while the isolation between the other ports varies between 7.8 and 8.9 dB for the measured values and 7.4 and 8.7 dB for the simulated values. How much the ports couple with each other will show itself to be important for the graceful degradation which will be discussed in 4.3.1.

The measured results from the fabricated structures and the simulated data are consistent except from some deviations that are most likely explained with the inexact method of assembly of the connector modifications.
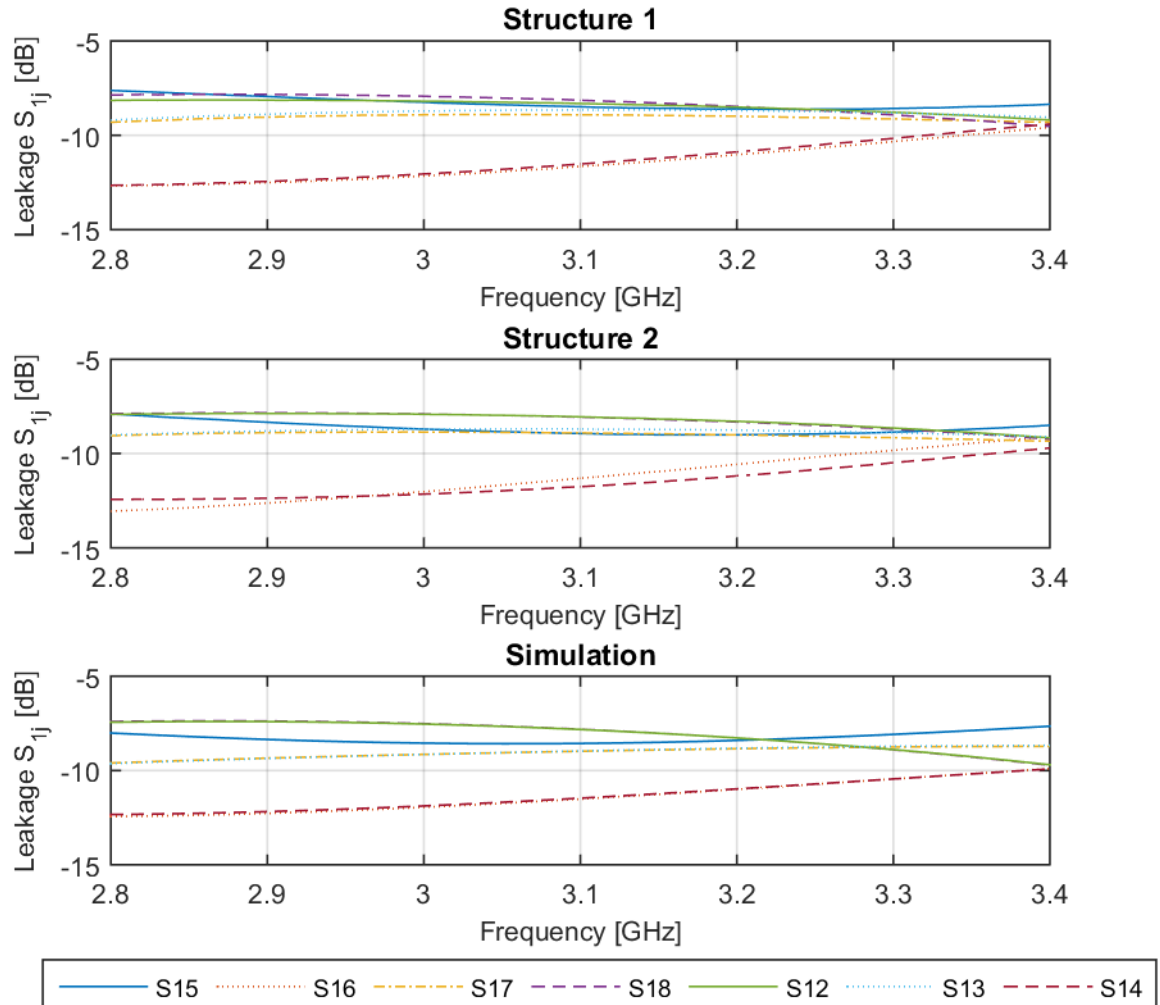
Figure 4-7. Measured leakage between peripheral ports for structure 1 and structure 2 and corresponding values from the simulated model. The best isolation is found between port 1 and 4 and port 1 and 6.

4.1.4 Sensitivity for Phase and Amplitude Variations

One of the benefits with radial designs is that all signals between the peripheral ports and the centre port should experience identical electrical path lengths due to the symmetry. In real life applications, imperfections in fabricated divider structures or amplifier circuits may cause variations in the input signal to the combiner. For radial cavity combiners, it is of interest to study the effect of unbalanced input signals to see whether the asymmetric behaviour in this case reduces the efficiency of the combiner.

The combiner sensitivity to these type deviations was studied by Monte Carlo simulations with 250 iterations in ADS. A Gaussian distribution was used for the phase and amplitude variation. The scattering matrix of the simulated structure was imported to ADS, and fed with eight input signals of P_{in}=1 dBm, which resulted in a combined output power of 10.012 dB at 3.1 GHz. The histograms in Figure 4-8 to Figure 4-9 below show the deviation from this output power $P_{out}[\text{dBm}] - P_{out,ref}[\text{dBm}]$ as the phase and amplitude is varied.

The losses are smaller than 0.1 dB for phase deviations up to ±5 degrees. Phase deviations of ±10 degrees results in losses up to 0.4 dB. This can be compared to the total back-to-back insertion loss of 0.2 dB from section 4.2.1. For low loss applications, phase variations of less than ±2 degrees should be required, since they cause power losses smaller than 0.015 dB according to the Monte Carlo simulation.
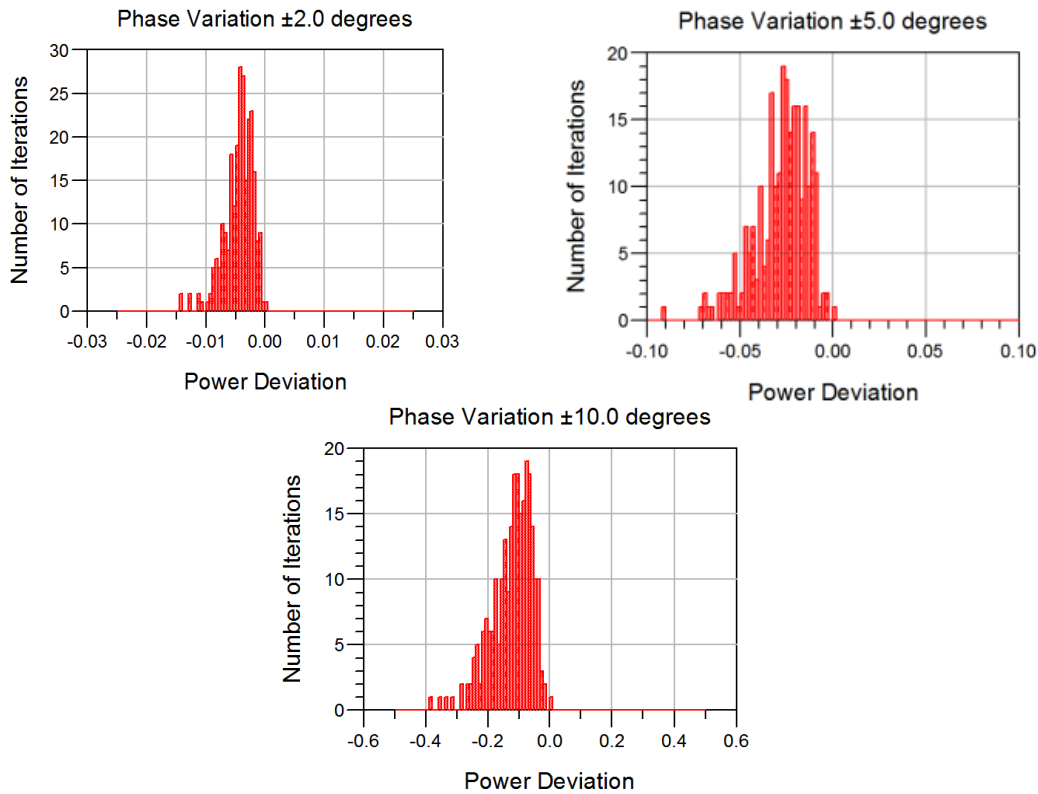
Figure 4-8. Histogram over the deviation in combiner power output for eight combined input signals of P_{in}=1 dBm with a phase deviation of ±2 degrees, ±5 degrees and ±10 degrees.

The histograms from the amplitude variations below differ from the ones from phase variations above, since they are symmetric around the 0 on x-axis. This means that variation in the amplitude of the input power does not appear to cause any losses in the combiner

structure, and the outcome of the Monte Carlo simulation corresponds to the variation of the input power.
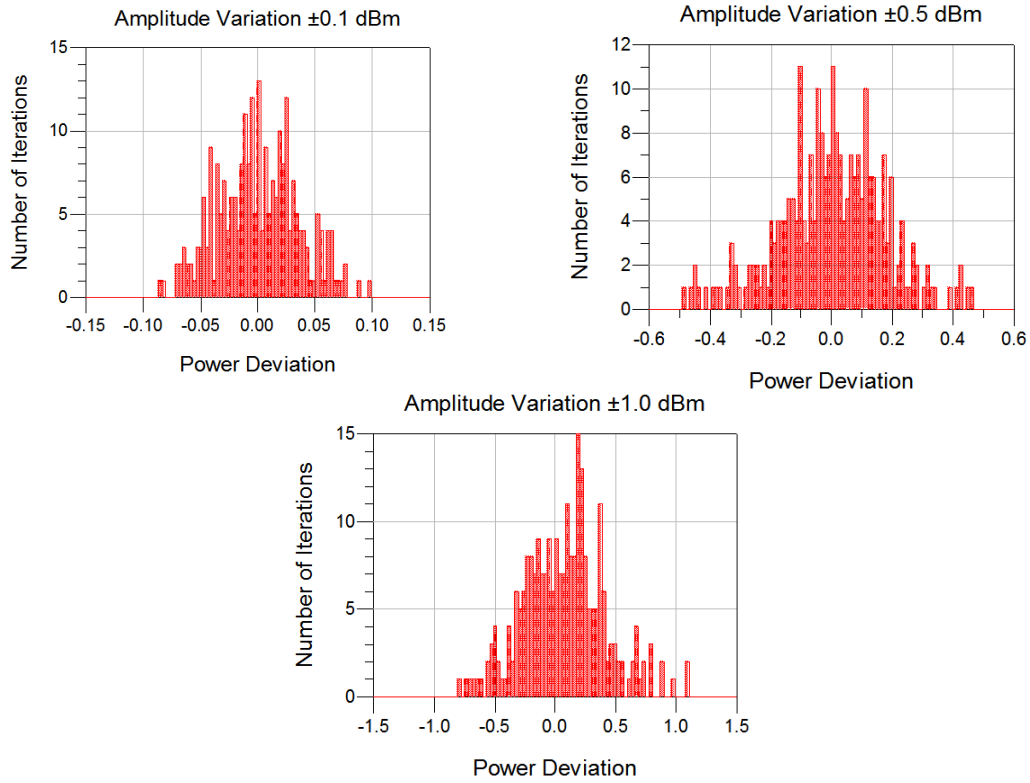
Figure 4-9. Histogram over the deviation in combiner power output for eight combined input signals of P_{in}=1±0.1 dBm, P_{in}=1±0.5 dBm and P_{in}=1±1 dBm.

4.2 Characteristics of Divider Connected to Combiner

A passive setup where structure 1 was used as a divider and structure 2 was used as a combiner was tested, to study the performance of the two structures like they are used in an amplifier system. The two structures were connected back-to-back, which means that they were connected to each other through their peripheral ports via SMA-adapters. The centre port at structure 1 was assigned to be port 1 and the centre port at structure 2 was assigned to be port 2. Since no adapters were included in the simulation, it was expected that reflections at additional frequencies could occur in the measurements compared to the simulation.
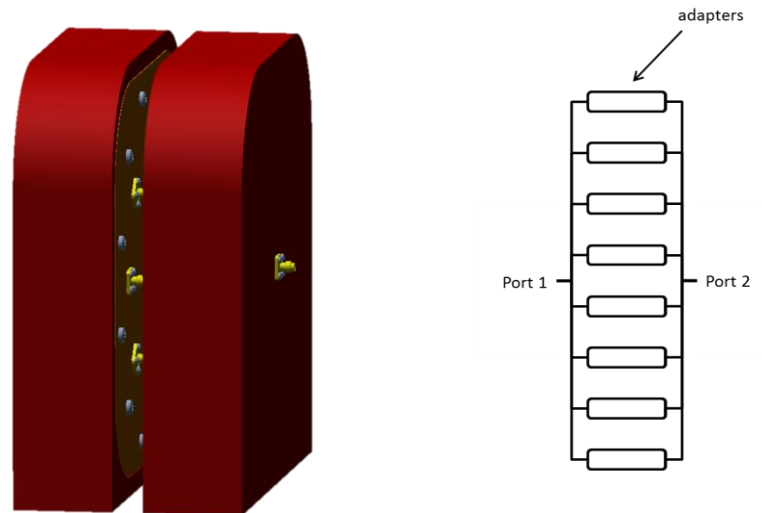
Figure 4-10. Back-to-back setup, where the peripheral ports of the two structures are connected through SMA-adapters

4.2.1 Scattering Parameters

The measured and the simulated results for the back-to-back setup are compared in Figure 4-11 below. The simulated and measured results have similar behaviours, but there seems to be a shift in frequency for the measured results compared to the simulated ones. A number of additional peaks are introduced in the measurements compared to the simulation, while the two significant peaks between 2.5 GHz and 2.8 GHz in the simulation are absent in the measurement. The reflection losses are higher in the measured data for the design frequencies, and the transmission losses between port 1 and port 2 increases from 0.05 dB to 0.28 dB at 3.1 GHz.
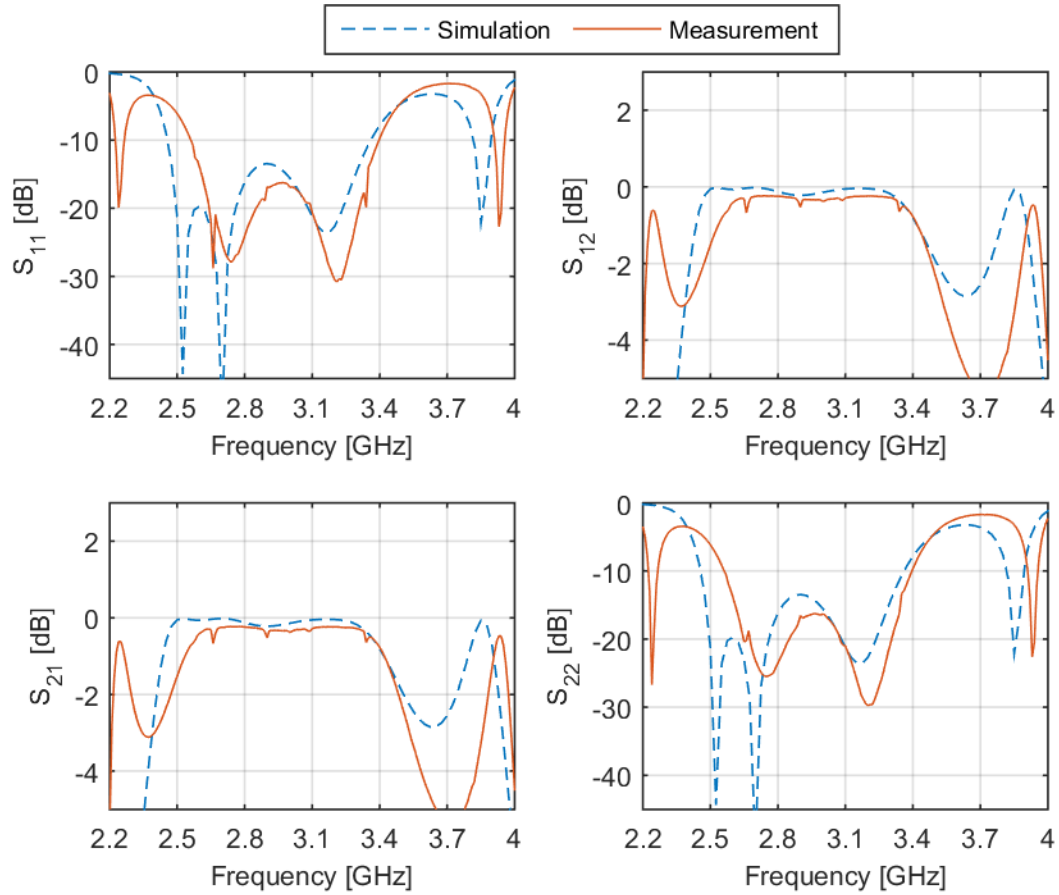
Figure 4-11. Scattering parameters from measurement and simulation of the back-to-back setup as seen in Figure 4-10.

4.2.2 Return and Insertion Losses

The return loss and insertion loss is by definition equal to S_{11} [dB] and S_{12} [dB] in Figure 4-11 respectively. The plotted data in Figure 4-12 shows the differences between the measurement and simulation in more detail. The return loss of the fabricated structures is up to 8 dB higher than the return loss of the simulated model, but also varies stronger within the design frequency band; from 16 dB to -30 dB. The RL=16 dB bandwidth is 0.7 GHz around 3 GHz, which gives a bandwidth of 24 %.

The insertion loss for the back-to-back setup suffers from discontinuities at 2.9 GHz, 3 GHz and 3.09 GHz. Since the peaks appears only for the back-to-back setup, and not in Figure 4-1 or Figure 4-2, a qualified guess is that they are a result of the addition of adapters to the structure. If they are ignored, an insertion loss of 0.29±0.05 dB applies for the design frequencies.
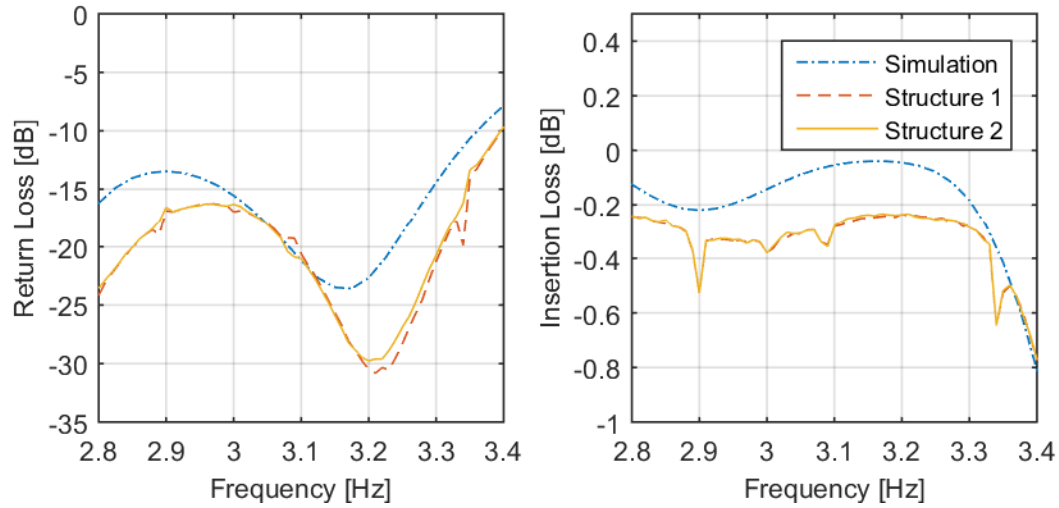
Figure 4-12. Return loss and insertion loss for passive divider-combiner combination. Both structure 1 and structure 2 are tested as divider and combiner respectively.

4.2.3 Broaband Filter Characteristics

The broadband filter characteristics of the back-to-back setup are studied to see if there are any unintentional passbands other than for the design frequencies. Frequencies corresponding to the harmonics of the amplifier that should be used in the active setup are of certain interest, to study whether a filter is needed at the amplifier output or not.

The transmission, S_{12}, is efficiently filtered out at the first harmonic around 6 GHz. At the second harmonic, around 9 GHz, there is a frequency band of approximately 9.2 GHz to 9.7 GHz where a signal can be transmitted with an insertion loss of -5 dB to -1 dB. Regarding the third harmonic, a relatively narrow peak in the transmission is seen just above 13 GHz (which is slightly higher than the theoretical third harmonic), with minimum insertion loss of 1 dB. No clear pass bands of transmission appear to exist for higher frequencies.
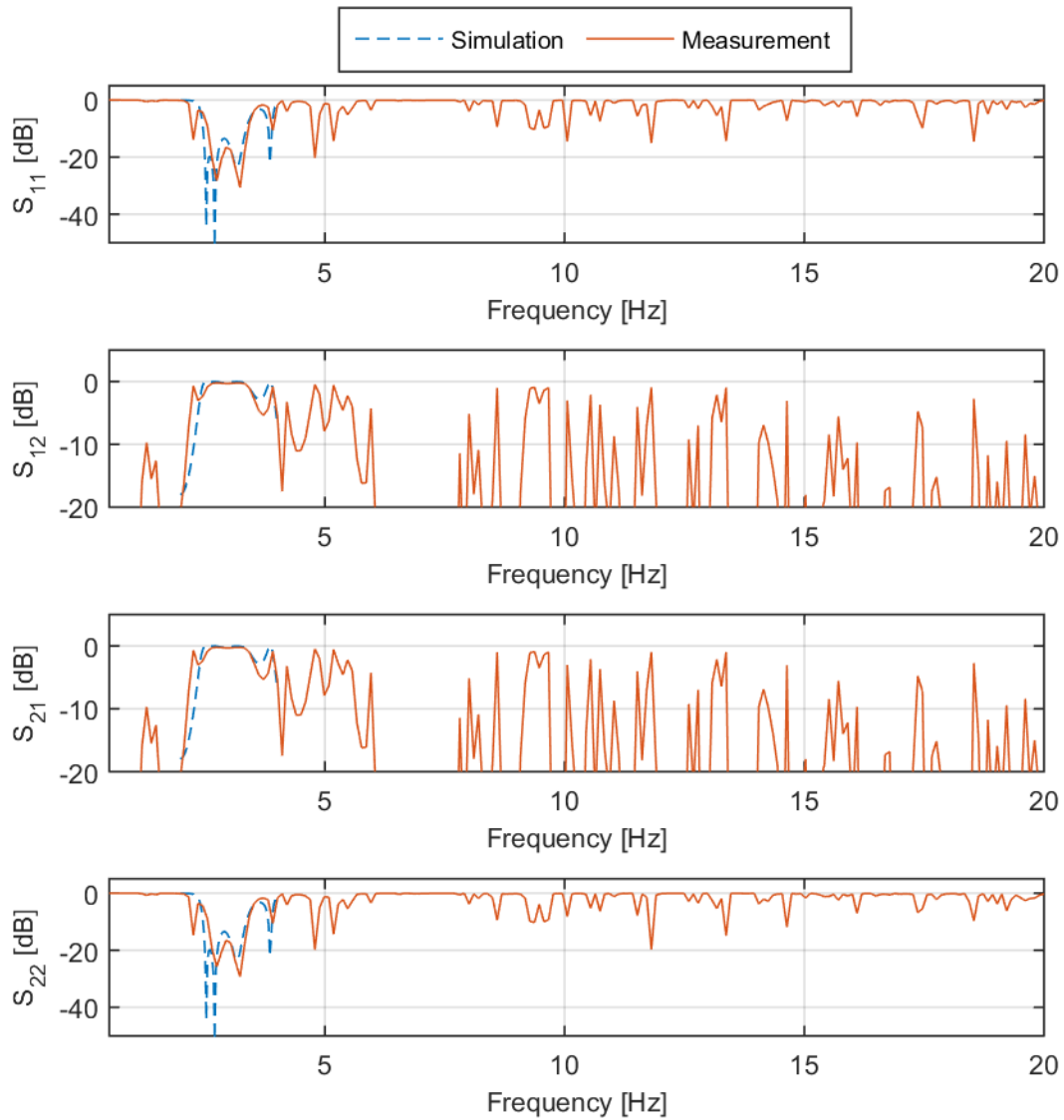
Figure 4-13. Broadband measurement of the back-to-back setup between 0.5 GHz and 20 GHz with simulated values as comparison for 2 GHz to 4 GHz.

4.3 Test Setup with Solid State Power Amplifiers

Eight InGaP HBT amplifiers are mounted between the peripheral ports in the back-to-back test setup. The amplifiers operate over DC-4 GHz with a typical gain of 11.7 dB [29]. Figure 4-14 shows the test setup. It is clear that the output power should equal the input power plus the gain of each amplifier minus the losses in the setup. This was verified and the characteristics of all power amplifiers were verified before the measurements began. All measurements in this section will be presented in relative gain, as the actual gain is not of interest for the functionality.
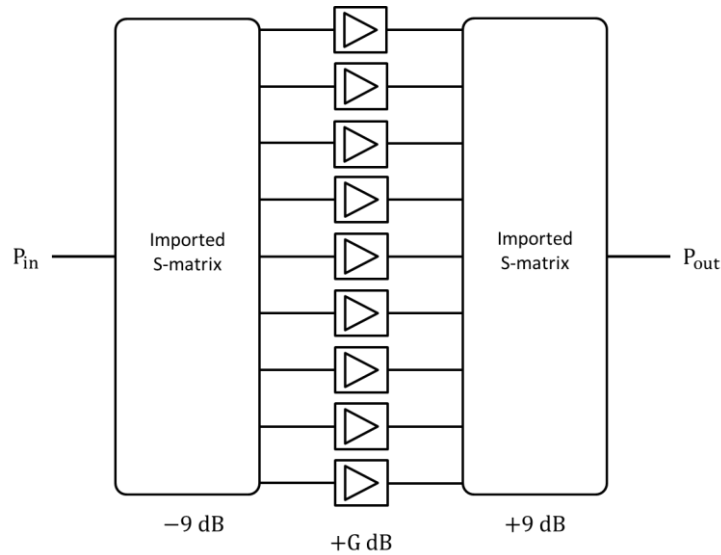
Figure 4-14. Schematic view of the active test setup where the peripheral ports of the structure are connected to solid state power amplifiers. The overall increase in P_{out} should be equal to the amplifier gain, G dB.

4.3.1 Graceful Degradation in the Event of Amplifier Failure

The measurement of graceful degradation was performed as follows: a reference measurement of S_{12} was done when all amplifiers were biased. After that, the bias was removed from one or more amplifier to imitate amplifier failure and the new S_{12} was measured. The results presented in Figure 4-15, Figure 4-16 and Figure 4-17 all show the change in gain that this results in.

Figure 4-15 shows the results for when the amplifiers are in their linear region. This means that when the power that should have gone through the unbiased amplifier is reflected and flows through other peripheral ports than the "failed" one, it may still get amplified and combined together with the rest of the output signal. In Figure 4-16, on the other hand, the amplifiers have been driven into compression so that the output from the amplifier is limited at its saturated output power. The result of this is that it does not matter if the power from a failed port is reflected and inserted into other amplifiers, since they are already at their maximum output power level. This can be seen when the results in Figure 4-15 and Figure 4-17 are compared.

The average power loss for 1-port failure in the saturated case results in a power loss of around 1.8 dB in average while the same scenario with amplifiers in the linear region results in a power loss of around 1.3 dB in average. The same difference for 2-port failures gives an average power loss of approximately 4 dB in the saturated case and 3 dB in the case where the amplifier operates in its linear region. It is clear from the measurements that the loss varies heavily with frequency, even over the relatively short band of design frequencies, 2.9 GHz to 3.3 GHz. The shape of the 1 port-loss curves are similar in the linear and saturated case, but the measurement from the saturated amplifiers appears to be shifted with approximately 50 MHz. This tendency is also seen in the 2-port failure data, but cannot be observed as clearly in the 3-port failure case since the saturated 3-port failure data does not have as noticeable peaks. The unevenness of the curve is discussed further in section 4.3.2.

Figure 4-15. The loss in gain as the bias is removed from a number of amplifiers when the amplifiers are in their linear region. "Port 1" in the legend means that the amplifier at port 1 is unbiased, "Port 1,5" means that the amplifiers at port 1 and port 5 are unbiased, and so on.

The loss that arises due to the removal of one of the ports in the combiner means that it is not possible to remove one port from the nearly ideal 8-port structure and acquire a nearly ideal 7-port structure. This is not very surprising considering the amount of optimization that was needed to design a well-functioning combiner/divider structure. As the impedance in one peripheral port is altered, all other ports will be affected since the impedance matching will no longer be valid. It is also possible that the uneven excitation of the cavity affects the resonant field in a way that no longer couples the peripheral ports to the centre port in the same way, as the symmetry of the structure is broken.

Figure 4-17 displays the simulated values of graceful degradation. The simulation was performed with measured parameters of the amplifiers in the linear region – biased as well as unbiased – and the scattering matrix from the designed structures. The measured scattering parameters from adapters, cables and attenuators in the measured test setup was also included in the simulation to reduce other differences between the measurement and simulation than those from the divider and combiner structures. The simulation show average losses around 1.3 dB for 1-port failures, just below 3 dB for 2-port failures and approximately 4-5 dB in the event of 3-port failures.
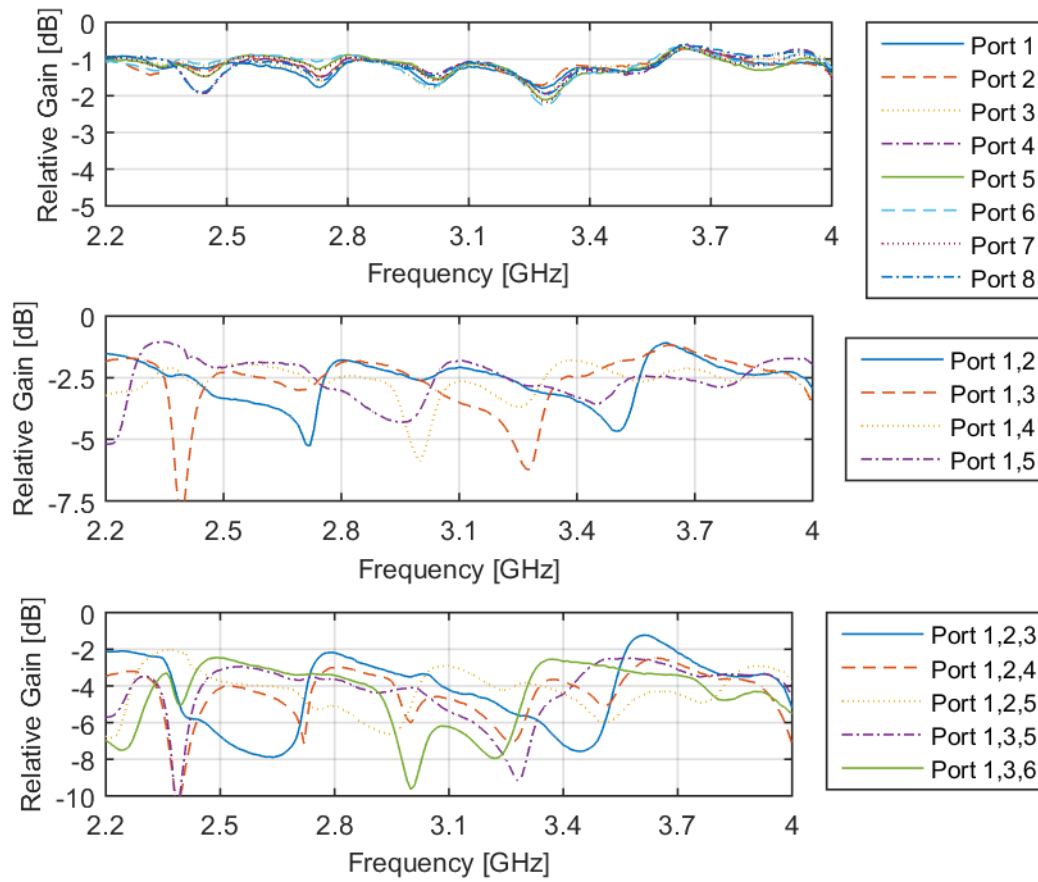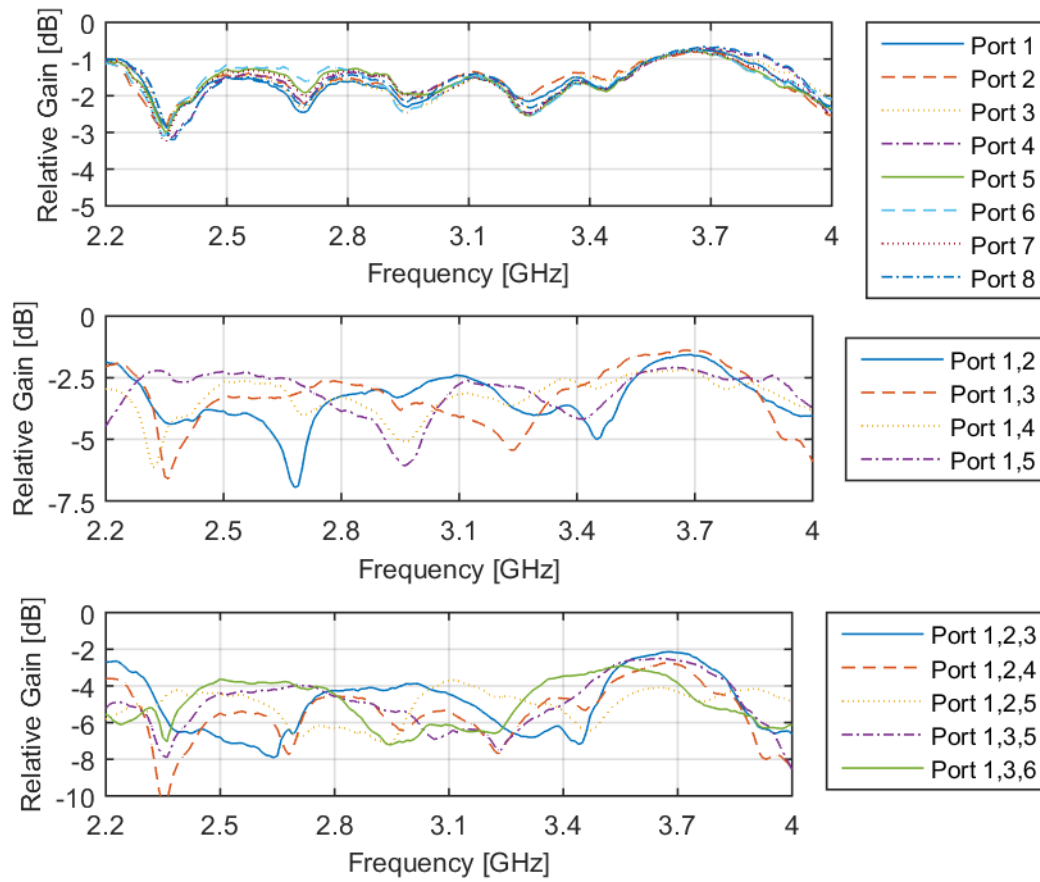
Figure 4-16. The loss in gain as the bias is removed from a number of amplifiers when the amplifiers are saturated. "Port 1" in the legend means that the amplifier at port 1 is unbiased, "Port 1,5" means that the amplifiers at port 1 and port 5 are unbiased, and so on.

The results agree with the measured results in the linear region. The simulated values are far more cohesive than the measured values, and since it is known from previous measurements that the peripheral ports suffer from asymmetry in the measured structures, it is a likely reason why.

From both the measurements and simulation, it is clear that failure of some ports or combinations of ports generate more losses than other – although it is much more obvious differences in the measured cases. One of the goals with the simulation and measurements was to understand why some cases offer a more graceful degradation than other and one hypothesis was that it could depend on the coupling between peripheral ports. It is hard to draw any conclusions from the results as they vary very much in frequency and since the simulated curves are so much flatter than the measured ones.
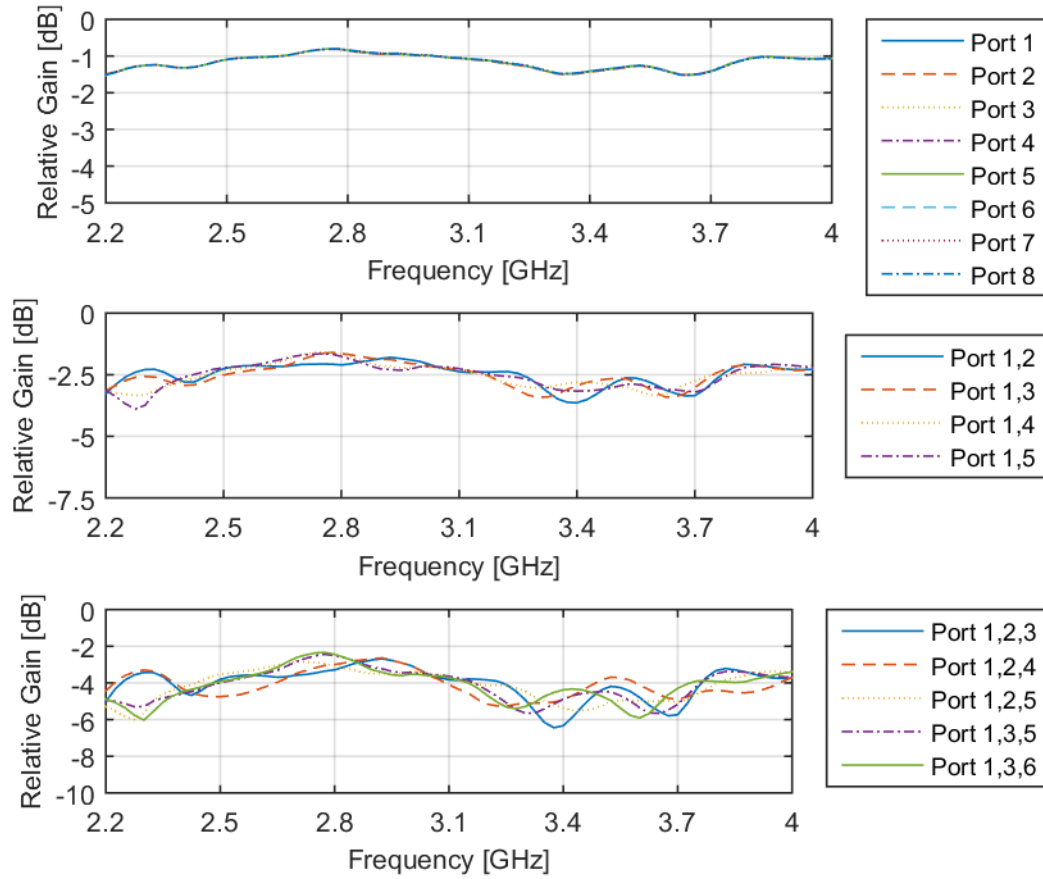
Figure 4-17. The simulated losses in gain as an amplifier taken out of operation. "Port 1" in the legend means that the amplifier at port 1 is unbiased ,"Port 1,5" means that the amplifiers at port 1 and port 5 are unbiased, and so on.

In conclusion, it can be stated that the loss that arises due to the removal of one of the ports in the combiner means that it is not possible to remove one port from the nearly ideal 8-port structure and acquire a nearly ideal 7-port structure. This is not very surprising considering the amount of optimization that was needed to design a well-functioning combiner/divider structure. As the impedance in one peripheral port is altered, all other ports will be affected since the impedance matching will no longer be valid. It is also possible that the uneven excitation of the cavity affects the resonant field in a way that changes the coupling of the peripheral ports to the centre port.

4.3.2 Methods for Improvement of Graceful Degradation

Even though graceful degradation is far better than total failure of an amplifier network if one of the constituent components fail, failure of one or more amplifiers still leads to a severe impairment of the functionality of the network. According to Ernst, Camisa and Presser [32] the decrease of output power for N-way combiners can be calculated as

$$\frac{P_{out}}{P_{out,max}} = \left[\sqrt{k} + \frac{M}{N}(1 - \sqrt{k}) \right]^2 \qquad (4.1)$$

where k is the fractional output of a failing amplifier, which varies between 0 and 1 depending on whether the amplifier fails entirely or not. M is the number of functioning amplifiers and N is the number of ports in the combiner network. For an 8-port combiner with one totally failed amplifier, (4.1) gives an output power of 77 % of the maximum output, which translates into a loss of 1.16 dB. The corresponding values for two failed amplifiers are 56 % and 2.5 dB and for three failed amplifiers: 40 % and 4 dB. This corresponds well to the measured and simulated results from the previous sections.

These theories are traditionally applied on tree structure combiner networks, which differ from the cavity combiners in their principle of construction. In this master thesis project, one of the aims was to study if there was a way to improve the graceful degradation by modification of the failed or remaining ports. In the event of one failed amplifier, it is a matter of trying to readjust the properties of the combiner so that it behaves more like a 7-way combiner than an 8-way combiner when it fails. This was done in the software ADS by replacement of one amplifier with different components or terminations according to the sketch in Figure 4-18.
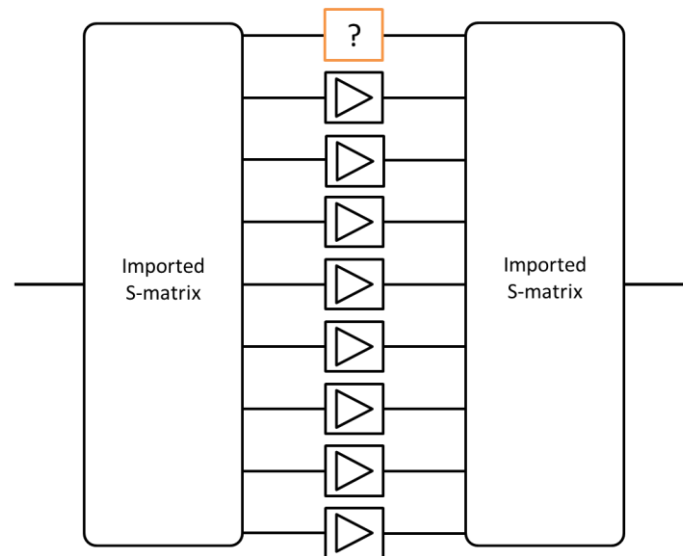
Figure 4-18. Network for test of methods for improvement of the graceful degradation. The box with the question mark was replaced with different type of terminations and components.

The removed amplifier model was replaced with open circuit, short circuit, a short circuit with an equation based 2-port Z-parameter component, a phase shifter, the scattering matrix measured from one unbiased amplifier and a combination of the latter and two equation based 2-port Z-parameter component – one at the input and one at the output ports of the scattering matrix. The circuits with the phase shifter and the Z-parameter components were optimized for maximum S_{21} between 2.9 GHz and 3.3 GHz and the resulting parameters are listed in the legend in Figure 4-19.

Figure 4-19 displays the resulting relative losses. It is clear from the results that different replacements for a faulty amplifier can change the graceful degradation for certain frequencies significantly. For example, to replace the amplifier with an open circuit leads to losses larger than 3 dB for some frequencies while a short circuit results in losses barely above 1 dB at the most, and with a more even behaviour over frequencies. The optimizations performed with the phase shifter and the Z-parameter components did not result in large improvements, but still affects the performance.
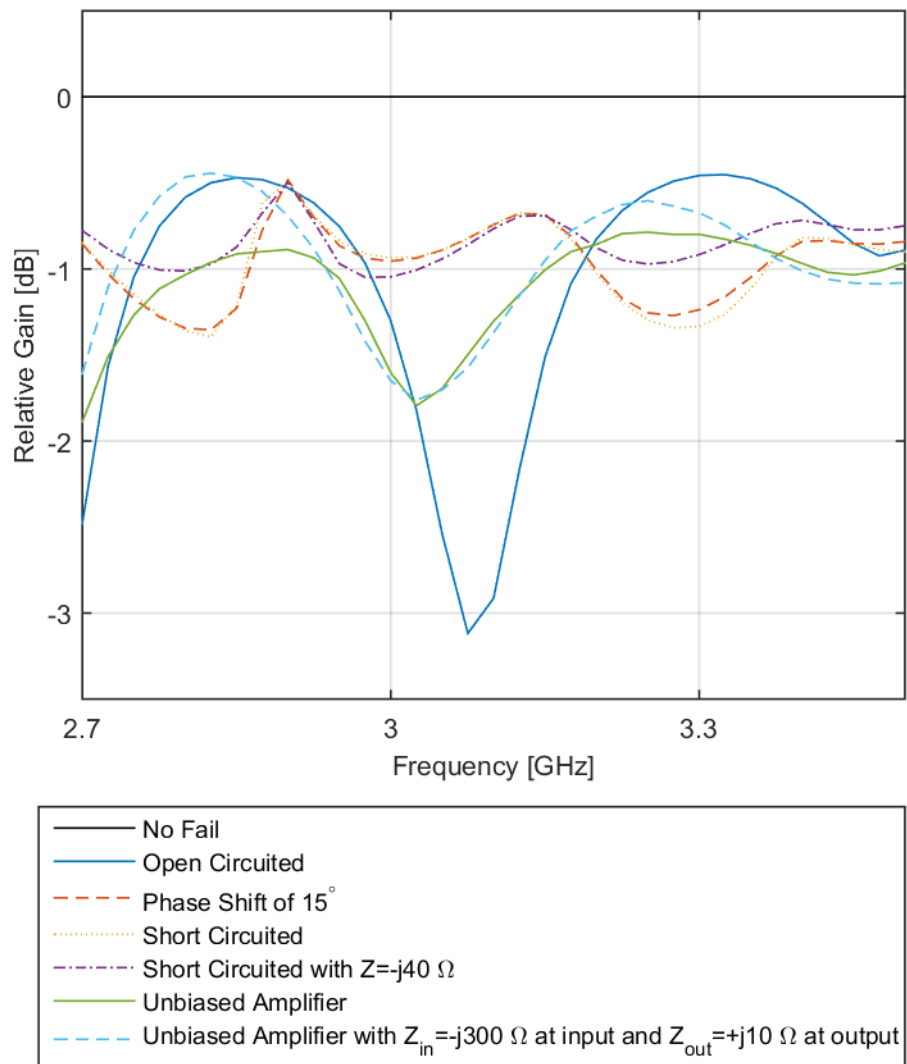
Figure 4-19. Result of the test of different ways to improve the graceful degradation. The best result for 2.9 GHz to 3.3 GHz is achieved when the failed amplifier is replaced with a phase shift of 15°.

Some tests to optimize different components at the remaining ports instead of the failed one was performed, but only for a passive combiner setup. That did not result in any successful improvements, but it could still be of interest to study possible optimizations further for the setup used in Figure 4-18, with the goal to find easy way to re-match the structures to behave more like (*N*-1)-way dividers and combiners in the event of a port failure.

5 DISCUSSION AND FURTHER WORK

5.1 Radial Power Combiner as an Alternative for Combiner Networks

The radial power combiner is very interesting as concept, as it is a relatively simple and robust way to realize high power generation with low losses. It has been investigated since the second half of the 20th century, but is despite this a relatively unknown and unused type of technology that may have many applications as the solid state power amplifiers continue to show increasing performance at high power levels.

5.2 Construction of Radial Cavity Power Combiners in General

In section 3.1, a study of the construction of a cylindrical cavity radial power combiner was presented. The aim of the study was not to go into detail of every design parameter as they change depending on the technology used to realize the cavity combiner. However, the goal was to give an idea about what challenges need to be dealt with in the design process, and what design considerations that need to be made in the beginning of a design process. In conclusion, there are four questions that one could ask oneself when designing a radial cavity combiner:

1. How many signals should be combined?

2. Are there any restrictions regarding choice of port interfaces?

3. How can the impedance for the different parts in the combiner be tuned?

4. Will there be need for additional isolation?

Some areas in the conceptual study should be studied further to get a better understanding of the construction, and most important of these are the restriction regarding number of peripheral ports and their positions. The number of ports is closely related to the bandwidth of a cavity combiner, but is also dependent on the required power level for the design.

Another interesting part of the construction is the isolation in a cavity combiner, which in all essential comes down to mode suppression of resonant modes in cylindrical cavities. Both the need of isolation and suitable ways to realize them are of interest. Usual tools for mode suppression such as slits where unwanted waves can radiate out or thin metal walls to block waves can be problematic in high power application.

5.3 Evaluation of the Design, Fabrication and Verification of the 8-Way Cavity Combiner/Divider Structures

All simulations and optimizations of the designed structures were performed in HFSS with all metal surfaces assigned as perfect electrical conducting surfaces and the cavity was assigned as vacuum. Apart from this, the only other material used in the simulations was the Teflon in the SMA connectors. When the fabrication of the combiner/divider structures was about to be initialized, a number of control simulations were performed. This included simulations of tolerances, possible leakage in joints and simulations of materials such as air, aluminium and

beryllium brass. None of these factors were considered to have high enough impact to be taken into consideration in the optimizations.

The copper cylinders that were used to modify the SMA connectors are the largest source of uncertainty in the realisation of the design. A large effort was made to simplify the assembly of them so that the result would be as precise as possible, and the prepared holes in the copper cylinders were designed to help fixating them in the correct positions. It was, despite this, hard to mount them identically and the incoherence in the reflection coefficient at the peripheral ports is most likely a result of this. The measured peripheral port return loss for the structures showed a significantly broader band than the simulation had predicted. This might be a result of the imperfect realization of the peripheral probe modifications.

The optimization of the probes and the cavity height gave satisfactory results, but the frequency bands with good matching at the peripheral and centre ports did not coincide. It would have been of interest to know if anything could have been done to have the best performance at both ports simultaneously without any trade-off with other design requirements. In order to get to the bottom of this, a more detailed analysis of the behaviour of the connector probe modifications needs to be performed.

5.4 Recommended Future Work

There are three main areas where further work would be recommended:

- Study of number of peripheral ports for cavity combiners and other types of radial combiners. Matsumura and Mizuno [9] discuss how the number of ports in a cavity combiner is related to the bandwidth and the choice of resonant mode for the cavity resonator, and their article is a good starting point for further work.

- Transformation of the cylindrical TM_{0m0} mode to a rectangular waveguide TE_{10} mode that would be of interest for the radar application. This is done in a number of published papers (see Table 2-3 for examples), but was not successfully done in this thesis work. A waveguide transducer could be used, but a probe that is excited by the cylindrical cavity and feeds the rectangular waveguide is another interesting option to study.

- Further studies of how the graceful degradation could be improved for different types of radial N-way combiners, with focus on how an N-way combiner can be modified into an (N-1)-way combiner in the event of port failure. It would be interesting to study how the reflected power from a failed port is distributed between the remaining ports, and how the matching of the remaining ports is affected. If the principle behind this is understood, it might be possible to draw conclusions about how the combiner should be modified to improve the graceful degradation.

5.5 Ethical Aspects and a Sustainability Perspective of the Radial Power Combiner/Divider

The radial power combiner/divider is used in the amplifier step of an RF system to generate high output power for satellite and radar applications. The technology would fill the same purpose that travelling wave tubes do today, meaning that there would likely not be any ethical consequences to consider regarding new innovations or applications of the technology.

An obvious advantage of amplifier systems based on SSPAs and radial power combiner/divider structures is the graceful degradation. When the technology is used in satellites for example, or research projects, it is not always possible to replace broken parts and failure of for example the TWTA could be the end of an experiment in space. If the output power is enough in the event of graceful degradation with an SSPA based amplification step, resources could be spared both financially and environmentally. The design of most combiner-based amplifier solutions is also constructed in a way that a minimum number of parts need to be exchanged in the event of failure which is also a responsible use of resources such as rare metals.

One application of the radial power combiner/divider is in military radar systems. The defence industry is not uncontroversial, and every technical invention in the area can be used in offence as well as defence. Radar systems can be used to detect threats and to support the elimination of them, but could also be used to detect targets and attack them. It is of course a subjective matter to decide who is suited to have weapons and other military equipment and why. These are very generic discussions and the technology of the SSPA and radial power combiner/divider system are not that specific to the area of application that these ethical aspects need to be considered. It is more correct to compare it to for example a bolt in a band waggon – it may be an essential part for the band waggons function, but it is also an essential part in many other uncontroversial inventions such as buildings, cars and Ferris wheels, and should therefore not be the subject for the ethical discussions surrounding the military industry.

6 CONCLUSION

The construction of a cylindrical cavity combiner/divider for the TM_{020} mode was analysed and a prototype 8-way combiner/divider structure was designed and fabricated. The most crucial part of the design process was the impedance matching at the different ports to reduce losses in the system. The measured average return loss for the peripheral ports is higher than 18.4 dB and the measured centre port return loss higher than 17.6 dB for a 10 % bandwidth around the centre design frequency of 3.1 GHz. The measured insertion loss is lower than 0.16 dB for the same band.

Uncoherent phase of the input power in a structure used as a combiner resulted in simulated losses; a phase variation of ± 2 degrees in the input signals caused loss in the combined power as large as 0.015 dB, while a phase variation of ± 5 degrees caused loss up to 0.1 dB, which is in the same size of the insertion loss. The combined output power was however unaffected by deviations in the amplitude of the input power.

The back-to-back structure showed decent filter characteristics but had tendencies to pass harmonics around 9.3 GHz.

The graceful degradation followed the theoretical model with some additional loss for the measurements and varied with frequency. Different methods to improve the graceful degradation were studied and improvements could be observed in some cases, but further studies are needed to draw any general conclusions.

BIBLIOGRAPHY

[1] R. Danieli and R. Giofré, "Development of High Efficiency and High LInearity Power Amplifiers for Space Applications," IEEE MTT-S Graduate Fellowship Project Report.

[2] A. Leggieri, G. Orengo, D. Passi and F. D. Paolo, "The Squarax Spatial Power Combiner," *Progress In Electromagentics Research C,* vol. 45, pp. 43-55, 2013.

[3] R. Giofré, P. Colantonio, E. Cipriani, F. Gianni, L. Gonzalez, F. D. Arriba and L. Cabria, "A High-Power Solid State Amplifier for Galileo Satellite System Exploiting European GaN Technology," International Journal of Microwave and Wireless Technologies, Cambrigde, 2016.

[4] K. J. Russel, "Microwave Power Combining Techniques," *IEEE Transactions on Microwave Theory and Techniques,* Vols. MTT-27, no. 5, pp. 472-478, 1979.

[5] C. G. Montgomery, R. H. Dicke and E. M. Purcell, Principles of Microwave Circuits, London: Peter Peregrinus Ltd., 1987.

[6] R. F. Harrington, Time Harmonic Electromagnetic Fields, New York: McGraw-Hill Book Company Inc., 1961.

[7] D. M. Pozar, Microwave Engineering, 4 ed., Oxford, UK: John Wiley & Sons, Inc, 2011.

[8] R. E. Collin, Foundations for Microwave Engineering, Hoboken: Wiley-IEEE Press, 2001.

[9] H. Matsumura and H. Mizuno, "Design of Microwave Power Combiner with Circular TM0m0 Mode Cavity," *Electronics and Communications in Japan, Part 2,* vol. 70, no. 9, 1987.

[10] M. Ghanadi, "A New Compact Broadband Radial Power Combiner," der Technischen Universität Berlin, Berlin, 2012.

[11] R. Aston, "Techniques for Increasing the Bandwidth of a TM010-Mode Power Combiner," *IEEE Transactions on Microwave Theory and Techniques,* Vols. MTT-27, no. 5, pp. 479-482, 1979.

[12] Y. Tokumitsu, T. Saito, N. Okubo and Y. Kaneko, "A 6-GHz 80-W GaAs FET Amplifier with a TM-Mode Cavity Power Combiner," *IEEE Transactions on Microwave Theory and Techniques,* Vols. MTT-32, no. 3, pp. 301-308, 1984.

[13] E. Belohoubek, R. Brown, H. Johnson, A. Fathy, D. Bechtle, D. Kalokitis and E. Mykietyn, "30-Way Radial Power Combiner for Miniature GaAs FET Power Amplifiers," *IEEE MTT-S International Microwave Symposium Digest,* pp. 515-518,

1986.

[14] K. Song, Y. Fan and Y. Zhang, "Eight-Way Substrate Integrated Waveguide Power Divider With Low Insertion Loss," *IEEE Transactions on Microwave Theory and Techniques,* vol. 56, no. 6, pp. 1473-1477, 2008.

[15] A. Jain, A. K. Gupta, D. K. Sharma, P. R. Hannurkar and S. K. Pathak, "Design and Analysis of a High-Power Radial Multi-Way Combiner," *International Journal of Microwave and Wireless Technologies,* vol. 6, no. 1, pp. 83-91, 2014.

[16] K. Wu, D. Deslandes and Y. Cassivi, "The Substrate Integrated Circuits - A New Concept For High- Frequency Electronics and Opto-Electronics," in *In proceedings of IEEE Telecommunications in Modern Satellite, Cable and Broadcasting Service*, Serbia Montenegro, 2003.

[17] J. M. Denoual, A. Peden, B. Della and J.-P. Fraysse, "16-Way Radial Divider/Combiner for Solid State Power Amplifiers in the K-band," in *Proceedings of IEEE 38th European Microwave Conference* , Amsterdam, Netherlands, 2008.

[18] H. Matsumura and H. Mizuno, "Design of Microwave Combiner with Waveguide Ports," *Electronics and Communications in Japan, Part 2,* vol. 71, no. 8, pp. 1279-1285, 1988.

[19] V. Ravindra, H. Saito, J. Hirokawa and M. Zhang, "Cylindrical Cavity Microwave Power Combiner with Microstrip Line Inputs and Rectangular Waveguide Output," in *IEEE MTT-S International Microwave Symposium*, Phoenix, Arizona, 2015.

[20] X. Shan, Z. Shen, P. Kumaresh and R. M. Jayasuriya, "A Novel 8-way Radial Power Combiner," in *Asia Pacific Microwave Conference*, Singapore, 2009.

[21] X. Li, G. Chen, M. Zhan and R. Xu, "A New Planar Compatible Power Combiner Based on Radial Waveguide," in *IEEE International Conference on Communication Problem-Solving*, Beijing, China, 2014.

[22] K. Song, Y. Fan and Z. He, "Broadband Radial Waveguide Spatial Combiner," *IEEE Microwave and Wireless Components Letter,* vol. 18, no. 2, pp. 73-75, 2008.

[23] Y.-J. He and Q.-X. Chu, "A Ka-Band Radial Power Combiner With Broadband Probes and Resisitve Slots," in *2016 IEEE International Workshop on Electromagnetics: Applications and Student Innovation Competition (iWEM)*, Nanjing, China, 2016.

[24] F. K. Gharekand, "Design of a 16 Way Radial Microwave Power Divider/Combiner with Rectangular Waveguide Output and Coaxial Inputs," *International Journal of Electronics and Communications,* vol. 68, no. 5, pp. 422-428, 2014.

[25] A. E. Fathy, S.-W. Lee and D. Kalokitis, "A Simplified Design Approach for Radial Power Combiners," *IEEE Transactions on Microwave Theory and Techniques,* vol. 54,

no. 1, pp. 247-255, 2006.

[26] D. I. D. Villiers, P. W. v. d. Walt and P. Meyer, "Design of Conical Transmission Line Power Combiners Using Tapered Line Matching Sections," *IEEE Transactions on Microwave Theory and Techniques,* vol. 56, no. 6, pp. 1478-1484, 2008.

[27] R. Faraji-Dana and H. Javadi-Bakhsh, "A Wideband Twenty-Element Microwave Spatial Power Combiner," *Scientia Iranica D,* vol. 21, no. 3, pp. 853-860, 2014.

[28] K. Song, F. Zhang, F. Chen and Y. Fan, "Wideband Millimetre-Wave Four-Way Spatial Power Combiner Based on Multilayer SIW," *Journal of Electromagnetic Waves and Applications,* vol. 27, no. 13, pp. 1715-1719, 2013.

[29] Mini-Circuits , "Datasheet for ERA 6+," 15 July 2016. [Online]. Available: http://www.minicircuits.com/pdfs/ERA-6+.pdf.

[30] R. J. Sullivan, Radar Foundations for Imaging and Advanced Concepts, Raleigh, NC: SciTech Pub., 2004.

[31] RND Connect, "Elfa Distrelec - Data Sheet for Male Connector SMA 50 Ohm Straight," [Online]. Available: https://www.elfa.se/Web/Downloads/_t/ds/rnd_205-00498_eng_tds.pdf?mime=application%2Fpdf. [Accessed 16 April 2017].

[32] R. L. Ernst, R. L. Camisa and A. Presser, "Graceful Degradation Properties of Matched N-port Power Amplifier Combiners," in *IEEE MTT-S International Microwave Symposium*, 1977.

APPENDIX A   Calculation of Resonator Impedance

From Montgomery, Dicke and Purcell[1], the input impedance for a cavity with an exciting iris aperture is

$$Z_{in} = Z_0 \tanh([\alpha + j\beta]l). \tag{A.1}$$

where α is the attenuation constant and β is the propagation constant. The propagation and attenuation constants are calculated as in Pozar[2]:

$$\beta = \sqrt{k^2 - k_c^2} = \sqrt{\left(\frac{2\pi f}{c}\right)^2 - \left(\frac{p_{nm}}{r_{resonator}}\right)^2} \tag{A.2}$$

$$\alpha = \frac{R_s(k_c^4 a^2 + \beta^2)}{\eta k \beta a (p_{nm}^2 - 1)} \tag{A.3}$$

where R_s is the surface resistivity, dependent on the permeability of the medium and the conductivity of the materials in the waveguide walls and η is the free space wave impedance. The variable l is the varied value of the height. Finally, Z_0 is the wave impedance in the cavity.
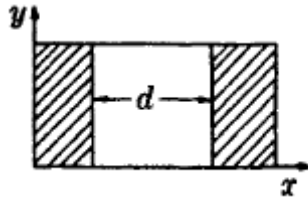
---

[1] C. G. Montgomery, R. H. Dicke and E. M. Purcell, Principles of Microwave Circuits, London: Peter Peregrinus Ltd., 1987.
[2] D. M. Pozar, Microwave Engineering, 4 ed., Oxford, UK: John Wiley & Sons, Inc, 2011.

APPENDIX B   Equivalent Circuit of Slits and Diaphragms in Waveguide-to-Cavity Ports

Montgomery, Dicke and Purcell [3] describe how thin metal sheets can be inserted in waveguides to introduce a shunt reactive element jB, when the thin metal sheets form a slit through which electromagnetic field can propagate. The orientation of the slit opening determines if the reactive element is inductive or capacitive; a slit parallel with the electrical field will give rise to a shunt inductance, a slit perpendicular to the electrical field will give rise to a capacitive impedance[3].

Slit parallel with the electrical field:

$$B = -\frac{\lambda_g}{a}\cot^2\frac{\pi d}{2a} + f\left(\frac{a}{\lambda}\right).$$

Slit orthogonal to the electrical field:
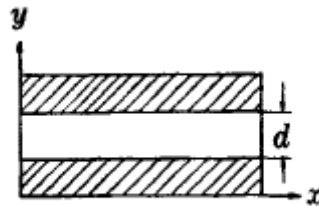
(a)

$$B = -\frac{4b}{\lambda_g}\ln\left(\csc\frac{\pi d}{2a}\right).$$

---

[3] C. G. Montgomery, R. H. Dicke and E. M. Purcell, Principles of Microwave Circuits, London: Peter Peregrinus Ltd., 1987.

APPENDIX C   Combiner Waveguide Output

A number of articles were studied to find interesting ways to tap out the combined signal through a waveguide. Some designs used circular waveguides since the cavity mode TM_{020} could easily excite the TM_{01} mode of the circular waveguide[4]. Other designs connected a rectangular waveguide directly to the cylindrical cavity[5].

The initial design idea was to create a circular-to-rectangular transducer. The circular waveguide radius was set by the frequencies of interest, while the length did not have any specific requirements. The rectangular waveguide dimensions were determined by the RSCS standard of WG10. A number of transducer designs were tested, where the one in Figure A-1. was the most promising one. The other tested designs had different rounding of the corners of the rectangular waveguides that couples with circular waveguide, different position and size of vertical slabs (or no slabs at all) and designs with Chebyshev transformation of the rectangular waveguide was also tested.
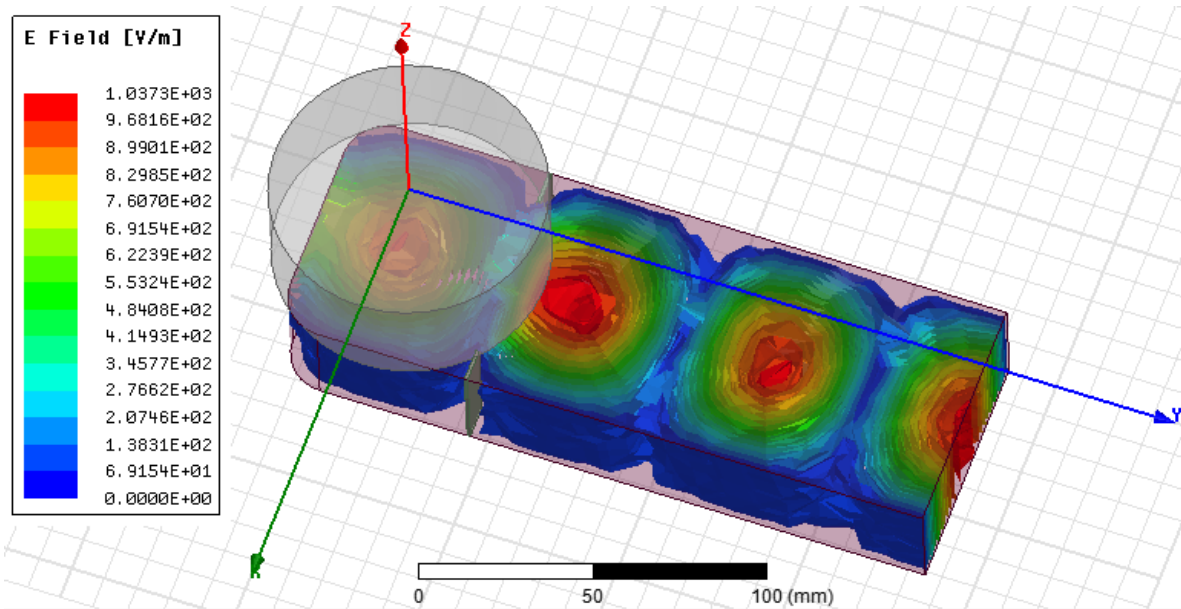

Figure A-1. Field plot of the transducer design to convert the circular TM_{01} mode to the rectangular TE_{11} mode.

---

[4] H. Matsumura and H. Mizuno, "Design of Microwave Combiner with Waveguide Ports," *Electronics and Communications in Japan, Part 2,* vol. 71, no. 8, pp. 1279-1285, 1988.

[5] V. Ravindra, H. Saito, J. Hirokawa and M. Zhang, "Cylindrical Cavity Microwave Power Combiner with Microstrip Line Inputs and Rectangular Waveguide Output," in *IEEE MTT-S International Microwave Symposium*, Phoenix, Arizona, 2015.
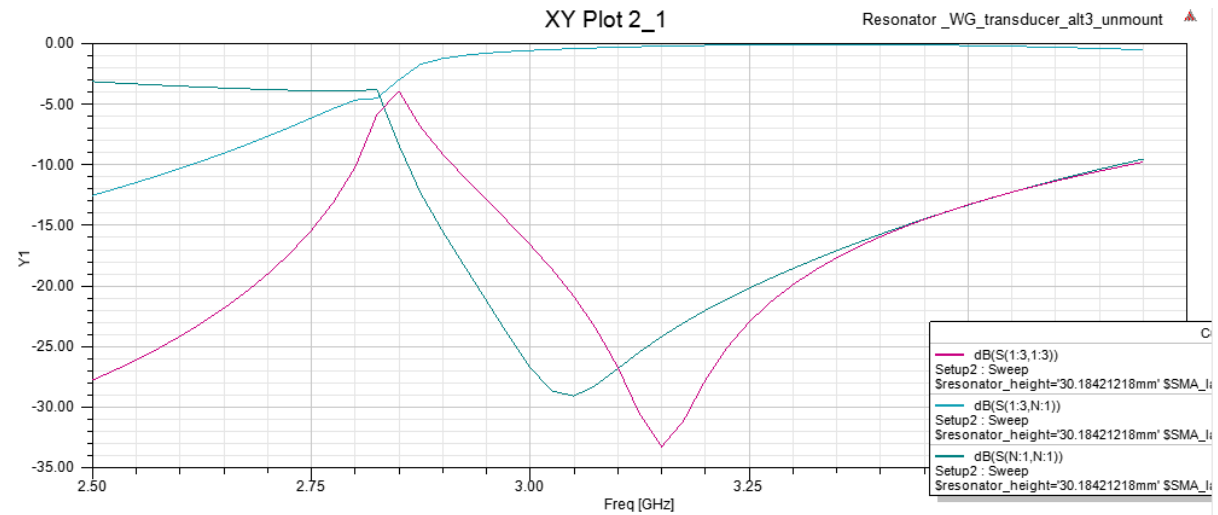
Figure A 2. Plotted input reflection coefficient at circular waveguide: dB(S(1:3),S(1:3)), output reflection coefficient at rectangular waveguide: dB(S(N:1),S(N:1)) and transmission dB(S(1:3),S(N:1)). The reflection coefficient is less than 9 dB for the input reflection coefficient and less than 16 dB for the output reflection coefficient for the range of 2.9 GHz to 3.3 GHz. The transmission losses are lower than 1.5 dB over the same range.
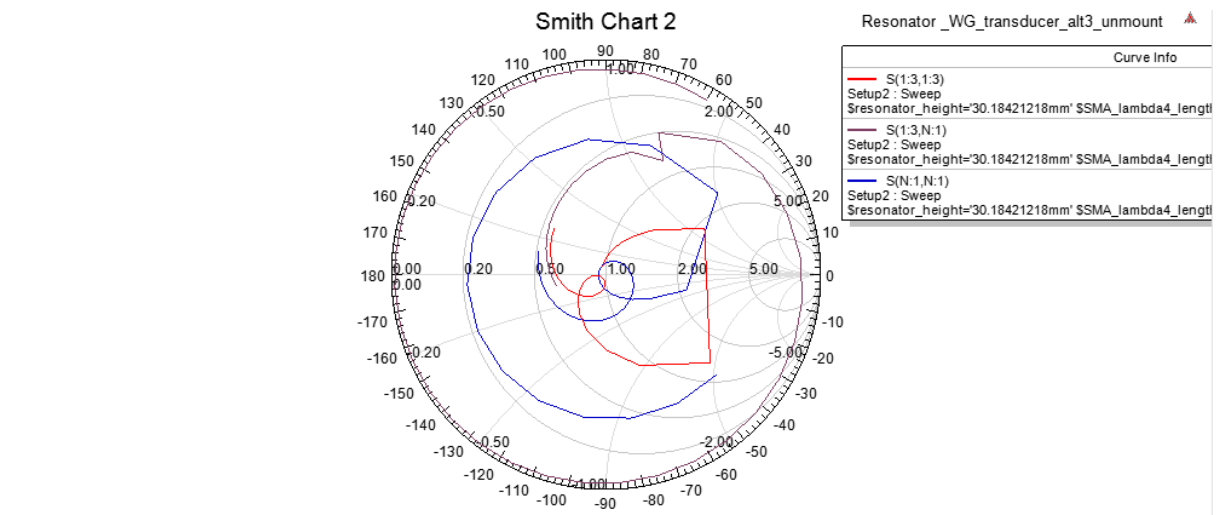

Figure A 3. Smith chart presentation of input reflection coefficient at circular waveguide: dB(S(1:3),S(1:3)), output reflection coefficient at rectangular waveguide: dB(S(N:1),S(N:1)) and transmission dB(S(1:3),S(N:1)).

An alternative solution is to use probe excitation of the rectangular waveguide, which can be realized in a number of ways[6]. This alternative was not considered within the scopes of this project but could be of interest to study in further work.

---

[6] F. K. Gharekand, "Design of a 16 Way Radial Microwave Power Divider/Combiner with Rectangular Waveguide Output and Coaxial Inputs," *International Journal of Electronics and Communications,* vol. 68, no. 5, pp. 422-428, 2014.

I